Dissolved Organic Matter and Associated Trace Metal Dynamics from River to Lake, Under Ice-Covered and Ice-Free Conditions

Worms, Isabelle; Chmiel, Hannah E.; Traber, Jacqueline; Tofield-Pasche, Natacha; Slaveykova, Vera

How to cite

WORMS, Isabelle et al. Dissolved Organic Matter and Associated Trace Metal Dynamics from River to Lake, Under Ice-Covered and Ice-Free Conditions. In: Environmental Science & Technology, 2019, vol. 53, n° 24, p. 14134–14143. doi: 10.1021/acs.est.9b02184

This publication URL: https://archive-ouverte.unige.ch/unige:131602
Publication DOI: 10.1021/acs.est.9b02184

Dissolved Organic Matter and Associated Trace Metal Dynamics from River to Lake, Under Ice-covered and Ice-free Conditions

Isabelle A. M. Worms[1], Hannah E. Chmiel[2], Jacqueline Traber[3], Natacha Tofield-Pasche[2] and Vera I. Slaveykova[1*]*

[1]Environmental Biogeochemistry and Ecotoxicology, Department F.-A. Forel for environmental and aquatic sciences, Earth and Environmental Sciences, Faculty of Sciences, University of Geneva, 66, boulevard Carl-Vogt, CH-1211 Geneva, Switzerland

[2] Limnological Center, Ecole Polytechnique Fédérale de Lausanne (EPFL), Station 2, 1015 Lausanne, Switzerland

[3] Process Engineering, Eawag, Überlandstrasse 133, 8600 Dübendorf, Switzerland

*corresponding authors

Key words: Humic substances; Metal dispersion; Asymmetrical Flow Field-Flow Fractionation ICP-MS; LC-OCD

ABSTRACT

The present study investigates the changes in dissolved organic matter (DOM) composition and its influences on trace metal dispersion from Shuya River (SR) in the Petrozavodsk Bay of Lake Onega during ice-covered and ice-free periods. Humic substances (HS) found in the SR dominated the composition of DOM through the river-bay-lake continuum in both periods. When the bay was ice-covered, both the aromaticity and the size of HS varied in the water column according to a horizontal stratification and decreased in the bay, while under ice-free conditions, they decreased along the river-lake gradient, suggesting in both cases the decrease in the proportion of HS with high aromatic character. These findings were associated to an overall decrease in the proportion of HS components that have the highest molecular masses. The quantification of metal bound to HS revealed that these characteristics were associated to a decrease in the binding capacity of the HS for Fe and Al, but not Cu while dispersing in the bay to the lake. Pb was found to bind on HS, but its behavior in the bay could not be related to the HS dispersion nor to the changes in HS properties.

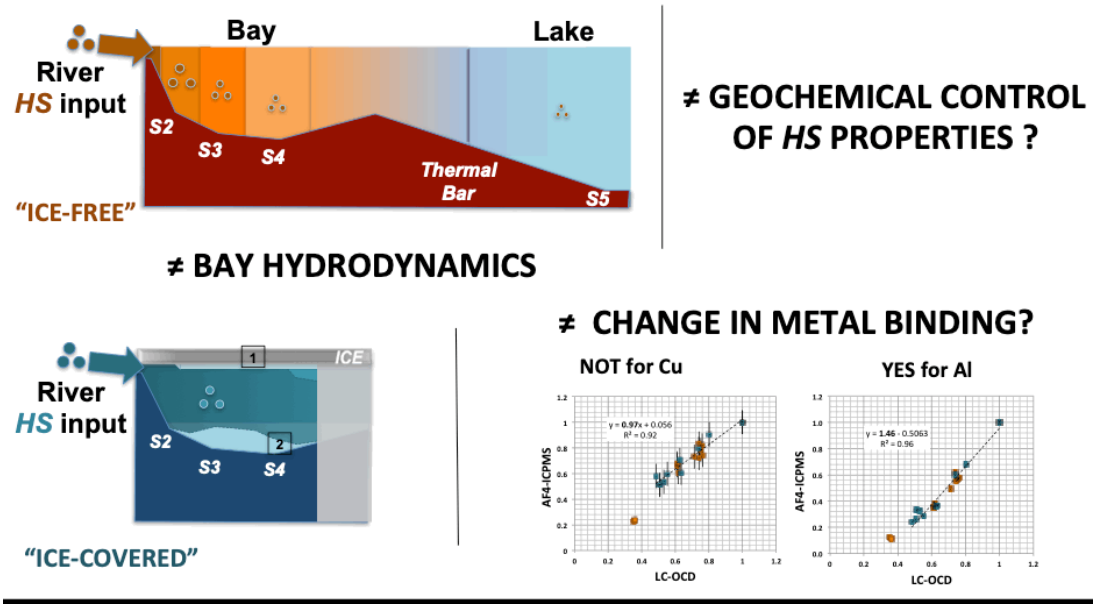

INTRODUCTION

Lakes are active sites for the transport, transformation, and storage of considerable amounts of carbon received from the terrestrial environment. Among dissolved organic matter (DOM) constituents, colloids (humic substances (HS), proteins, polysaccharides…) are important mediators in metal partitioning between truly dissolved (ionic or small metallic complexes < 0.3 kDa) and particulate phases (larger components binding metals > 1 μm) e.g. by working with inorganic colloids as "colloidal pumps".[1]

HS and colloidal mineral oxides are also known to act as carriers for trace metals dispersion in diverse aquatic environments. Prior studies using flow field-flow fractionation[2-6] suggest that some trace metals preferentially bind with inorganic colloids (iron/manganese). In addition, natural inorganic colloidal material in the smallest size range (< 20 nm) significantly influenced the interactions of metals such as Pb[7, 8] or As[9] with HS, however have no effect on Cu[7, 8, 10] in riverine systems. The behavior of metals associated with these small colloids is affected by ferrihydrite solubility and coagulation, both of which depended on environmental variables such as pH, ionic strength, temperature, pO_2 and Fe/DOM ratio.[7, 9, 11] Besides, the nature and properties of DOM also affect the behavior of iron colloid formation,[12] and their stability in aquatic media.[13-15]

Largely dependent on seasonal hydro-chemical features, both DOM and iron oxide pumps can control the cycling of trace elements in boreal lakes and catchments following changes in lake stratification and hydrochemistry.[16, 17] For example, a decrease in colloidal DOM from 75% to 20% in a large humic lake was previously reported to affect the proportion of colloidal Cu, Zn, Cd, Ni, Fe, Cr, Mn, Co and Pb.[18] In addition, the autochthonous production of high molecular mass organic compounds such as polysaccharides was shown to stabilize both colloidal Al and Fe,[19] for which the further agglomeration by inter-molecular bridging and removal depend on the electrolyte cations concentrations.[20, 21] All of these mechanisms were

shown to be responsible for major changes in the distribution of metals within the colloidal pool but were shown to occur in lakes with high biological productivity during summer time and/or when photo-alteration played a role in HS degradation.

The composition of aquatic DOM thereby influences the transport and the removal of trace elements,[22-25] the bioavailability of micronutrients or toxic metals[26, 27] and the cycling of organic carbon.[28]

Although the dynamics of DOM is relatively well-studied in marine estuaries,[29, 30] the changes in DOM nature and size distribution that occur in lake watershed transition zones has obtained little attention. A recent study on the dispersion of riverine DOM in Lake Michigan revealed the importance of conductivity in modulating its size distribution and composition.[31]

In spite of the above-mentioned advancements, the role of small colloidal pool dynamics in metal dispersion from rivers to lakes still requires elucidation especially during the winter period.

The present work provides new insights on the dynamics of DOM in northern humic-rich lake watershed and on its effects on the dispersion of metals under ice-covered and ice-free conditions. We focused on Petrozavodsk Bay in Lake Onega, which receives water from the Shuya River. The specific aims are to: (i) follow changes in DOM composition, chemical properties and molar mass through the river-lake continuum; (ii) examine how humic bound metals (M-HS) that originate from river behave in the transition zone; and (iii) assess if the iron-oxide colloidal stability can influence the dispersion of HS and their associated metals.

MATERIALS AND METHODS

Sampling sites description and water samples collection

Lake Onega is the second largest lake of Europe and located in North-Western Russia at a latitude of 61 to 63 °N (Republic of Karelia). The major inflows are Vodla, Shuya, and Suna

89 Rivers that account for 60% of the total inputs to the lake (17.6 km^3 yr^{-1}). This large
90 dystrophic lake has a surface area of 9'720 km^2 and a volume of 295 km^3, with a water
91 residence time of 15.6 years.[32] The Petrozavodsk bay is situated in the Northwestern part of
92 Lake Onega and has an area of 73 km^2 and water volume of 1.17 km^3.[32] The Shuya River is
93 the largest tributary of the Petrozavodsk Bay with a mean annual runoff of 3.12 km^3 $year^{-1}$,
94 corresponding to 93% of the total flow volume. The geochemistry of the bay is determined by
95 the mixing of tributaries (river, precipitation, drainage and subsurface) and lake water[33, 34] and
96 have an annual water exchange period of 1.6 months.[35] Two sampling campaigns were
97 organized to compare ice-covered and ice-free conditions. Several sampling sites were
98 chosen along the river-bay-lake transect: Shuya River mouth (SR), 3 stations in the
99 Petrozavodsk Bay (S2, S3, S4) and one station in the central part of Lake Onega (S5) for June
100 (**Figure 1**, **Figure S1**).

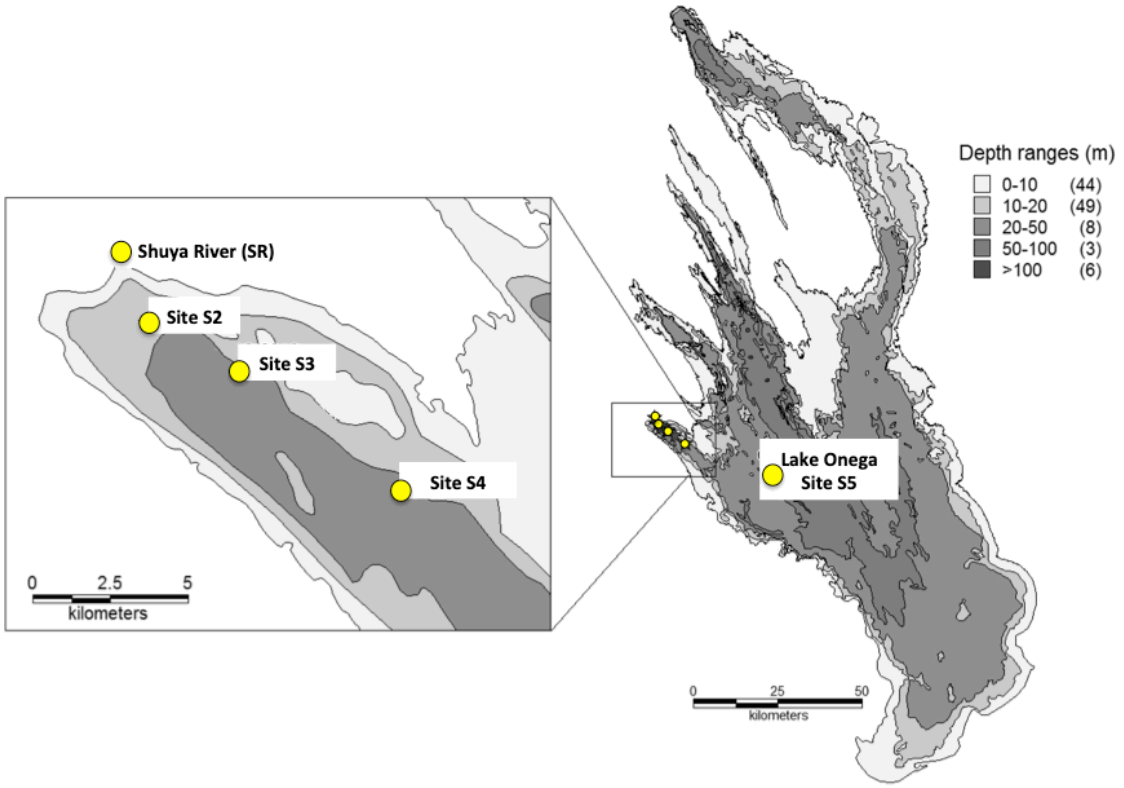

Figure 1. Cartography of the sampling sites from the Shuya River mouth (SR) through the Petrozavodsk Bay (Site S2, Site S3, Site S4) to Lake Onega (Site S5). The exact coordinates can be found in **Table S1**.

101

102 The physico-chemistry of the watershed area is described in other studies during the same
103 sampling campaigns or previous expeditions[36-41] and summarized in **Figure S1**. Briefly, under
104 ice-covered conditions the mixing of SR with the lake water is controlled by the convection
105 promoted by the light within the thin under-ice water layer (referred as *surface depth* after,
106 **Figure S1 A**). The convection depth varied during our sampling campaigns between 11.1 and
107 19.5 m.[36] A thinner convectively mixed layer (CML) related to river intrusion at bottom of the
108 CML (*intermediary depth*),[36, 38] and just above the warmer inversely stratified layer (*bottom*
109 *depth*, **Figure S1 B**) were also shown. An intermediate situation should have occurred at the

time we sampled considering the relatively high river discharge (38 m^3 s^{-1}) and the thin snow-cover.[36, 42] Under ice-free conditions, the bay is characterized by a decrease in temperature (6.5°C) before reaching a thermal bar (4°C) located at 30 km from the river mouth (9.2°C) that limited the water exchange with the cold lake (2.5°C).[41] Lake Onega was sampled at the Site S5 located at 45 km from the river mouth (**Figure 1 and Figure S1**). The monthly water discharge was 217 m^3 s^{-1} in June 2017.

At each site 2.0 L of water were sampled at the three different layers characteristic of winter stratification under ice-covered conditions (*surface, intermediate, bottom*) and at three different depths in the water column under ice-free conditions (**Table S1 and Figure S1**). Water was then filtered on-site through a Nalgene filter unit using a regenerated cellulose membrane filter with 0.45 μm cut-off (Millipore, 47 mm), pre-washed in 1% HNO_3 (v/v). The filtered water was held at 4°C in 2.0 L PET bottles that were pre-washed with 1% HNO_3 and stored in the dark prior further characterization.

Determination of DOM bulk characteristics

The bulk characteristics of DOM were evaluated by measuring DOC (Shimatzu TOC-5000A (Kyoto, Japan)) and determining biological (BIX), humification (HIX) and fluorescence indexes (FIX) from fluorescence emission excitation matrices (EEMs) obtained by LS 55 Luminescence Spectrometer (Perkin-Elmer) as detailed in the SI.

Characterization of the organic matter composition and molecular mass by liquid chromatography - organic carbon detection (LC-OCD)

Hydrophilic organic matter (HydOM) components, biopolymers (BP), humic substances (HS), building blocks (BB), low molecular mass humics or acids or neutral compounds (LMH, LMA, LMN) were quantitatively measured in each samples by size exclusion

chromatography using Toyopearl® HW-50S column (Tosoh Bioscience) with 24 mM phosphate buffer at pH = 6.6 as eluent.[43] Molecular mass distribution parameters of the HS fraction and their associated specific UV absorbance (HS-SUVA), were derived according to ref [43]. Further details can be found in the **SI**.

DOM and associated metals fractionation analysis by Asymmetrical flow field-flow fractionation (AF4) coupled to diode array, fluorescence and ICPMS detectors

Size fractionation of DOM and colloids (< 0.45 μm) was carried out using the same set-up than we previously described,[44, 45] and detailed in SI. The ICPMS signals were processed using Origin®Pro2017 (OriginalLab) with a testing license kindly provided by ADDITIVE GmbH, in order to quantify the metal bound to HS (M−HS) by deconvolution including small iron-oxide clusters (SCIox). The M−HS concentrations and carbon contents of the humic substances obtained by LC-OCD were correlated after normalization to the values obtained for SR (M−HS/ $M-HS_{SR}$ and C−HS/ $C-HS_{SR}$ respectively). Hence, only the dispersion and not inter-seasonal variability of the river inputs on the binding capacity can be followed directly.

RESULTS AND DISCUSSION

DOM bulk characteristics and composition

All samples were characterized by quite high DOC concentrations typical for humic-rich waters of the boreal forest areas, and the Karelian region.[46] The DOC values obtained for the Shuya River water were comparable in March and June (**Figure 2**), and are attributed to peatland that the river drains.[46] In March, the DOC dispersion was in agreement with river intrusion at the bottom of the intermediary layer with slight exchange with the bottom layer and an apparent DOC depletion in the shallowest depth sampled at 0.5 m of the ice cover for

160 sites S3 and S4 **(Figure 2 A, B)**.[38] Under ice-free conditions, the continuous vertical
161 temperature gradient took place.[41] Thus a decrease in DOC concentrations from the SR
162 towards the central lake was apparent through the bay (**Figure 2 A, B**) without stratification.
163 In Lake Onega at site S5, DOC reached values of 6.5 mg L^{-1}, similar to those obtained in June
164 2016 denoting its inter-annual stability.[37]

165 The SUVA for the SR samples was higher under ice-covered conditions as compared with
166 samples from ice-free conditions (**Figure 2 C, D**). The values obtained were above those
167 generally found for freshwaters (SUVA around 3)[47] and suggested a high proportion of
168 chromophoric components in DOM. The SUVA values decreased while the river water was
169 reaching the bay and were close to 3 L mgC^{-1} m^{-1} in the open lake. Such a progressive loss in
170 SUVA values of DOM indicated a loss of aromaticity of the chromophoric components[48]
171 through river–lake gradient.

172 The high values of SUVA strongly suggested an important input of humic substances by the
173 SR into the bay. In line with these results, EEM fingerprints are characterized by the presence
174 of the main fluorescence peaks corresponding to humic-like fluorophores (A, C). The absence
175 of protein-like fluorophores (T) suggests that the contribution of microbial production of
176 organic matter was negligible (**Figure 2**).[49] This pattern was conserved with dilution through
177 the bay and in the open lake, in ice-covered and ice-free conditions (**Figure S2**).

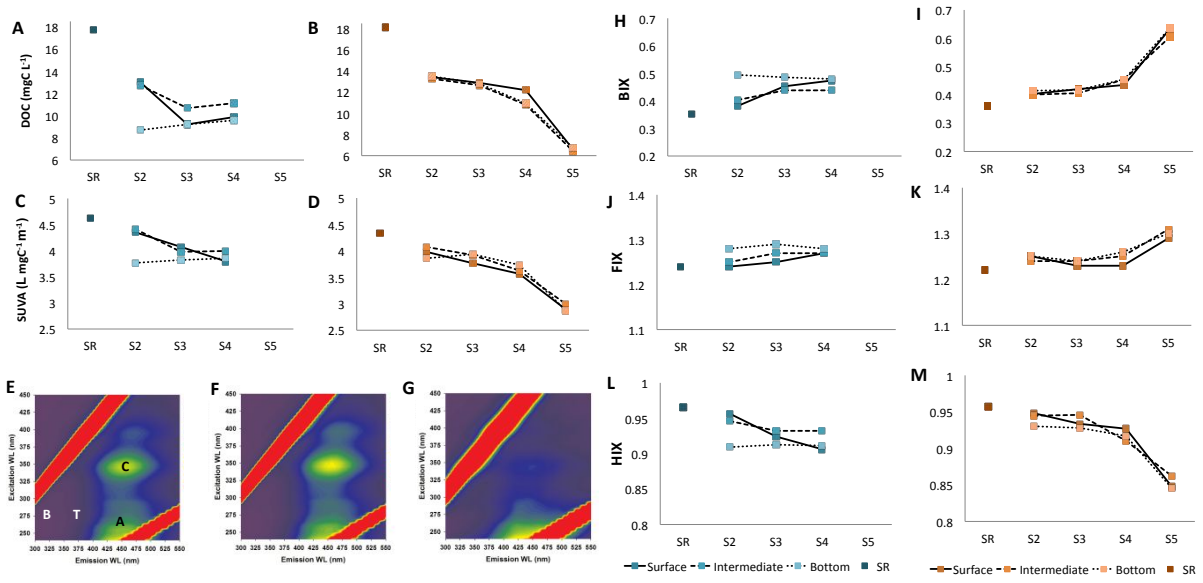

Figure 2. Evolution of bulk properties DOM in the river–bay–lake Onega continuum under ice-cover (blue) and ice-free conditions (orange). Dispersion profiles from Shuya River (SR) through the Bay (S2, S3, S4) and in the central lake (S5) at different depths (Surface = plain lines, Intermediate = dashed lines and Bottom = dotted lines of dissolved organic carbon (A, B), specific UV absorbance (SUVA, C, D), EEM fingerprints for ice-covered (E) ice-off (F) Shuya river and Lake (G), and dispersion profils for associated fluorescence characterisation of DOM (BIX[50], J, K FIX[51], L, M and HIX [S52]). Lake Onega sampling site S5 was inaccessible in March 2017. Peaks A ($\lambda_{ex/em}$ = 350 nm/450 nm), C ($\lambda_{ex/em}$ = 250 nm/450 nm), humic-like fluorophores and B and T ($\lambda_{ex/em}$ = 280 nm /300-375 nm) protein-like fluorophores[49]

178

179 The biological index (BIX) (**Figure 2 J, K**; indicator of fresh autochthonous DOM if > 1),[50]
180 humification index (HIX) (**Figure 2 L, M**; related to the condensation degree of HS) and
181 fluorescence index (FIX)[51] were also affected by differences in seasonal stratification of the
182 Petrozavodsk Bay. For SR samples BIX were of 0.35 in both March and June, suggesting low
183 contribution from freshly derived microbial DOM. The BIX values increased in Petrozavodsk
184 Bay and rise to 0.7 in the central lake with no apparent depth dependency, largely explained
185 by the gradual vertical mixing of the river and due to the limited primary production of
186 autochthonous DOM in the bay [39] and Lake Onega.[53] These results are in line with FIX
187 values typical for HS from pedogenic origin.[51] The HIX values for the Shuya River are equal
188 to 0.97 suggesting a high degree of unsaturation[52, 54] and are higher than humic isolates or
189 natural freshwaters, which have maximal HIX values near 0.94.[47] The values of HIX

190 progressively decreased with the distance of the river mount reaching values close to 0.9. In
191 the central lake, the values around 0.85 suggested a loss of aromaticity. The measured HIX
192 values were however larger than 0.6−0.7, a characteristic range for microbiologically derived
193 DOM. Together with low BIX (and overall low FIX values), this suggests that the decrease in
194 the DOM aromaticity through the bay was not due to the contribution of more freshly formed
195 microbial HS.[55]
196 The LC−OCD measurements confirmed that the DOM in SR, Petrozavodsk Bay and Lake
197 Onega was dominated by a high proportion of HS (**Figure 3**). The fraction of HS was
198 comparable in the different sampling sites of Petrozavodsk Bay with lowest value found at the
199 bottom of the bay under ice-covered conditions. Under ice-free conditions, HS accounted for
200 74.7−79.0% in the bay and decreased in the lake. The biopolymer components represented
201 only < 3.2% of the hydrophilic organic matter and neutrals ranged between 5.4 and 7.7% at
202 all the studied sites and seasons, in agreement with low (or no) autochthonous DOM
203 production shown by BIX and HIX measurements (**Figure 2**). The proportion of HS building
204 blocks (BB) varied between 10.0 and 14.0% in samples from the March campaign, with the
205 highest values found at the bottom of the bay. In June, BB varied between 8.8 and 13.9%
206 with higher proportions in the lake.
207 Humic substances are formed by collections of diverse, relatively low molecular mass
208 components (e.g. BB, LMW) forming dynamic associations, stabilized by hydrophobic
209 interactions and hydrogen bonds, and capable of organizing into a supramolecular structure in
210 suitable aqueous environments.[56] Therefore, different proportions of BB suggested
211 differences in the agglomeration states of the humic components especially at the bottom
212 layer under ice-covered conditions and in the lake that could be related to the lower aromatic
213 character measured at these locations.
214

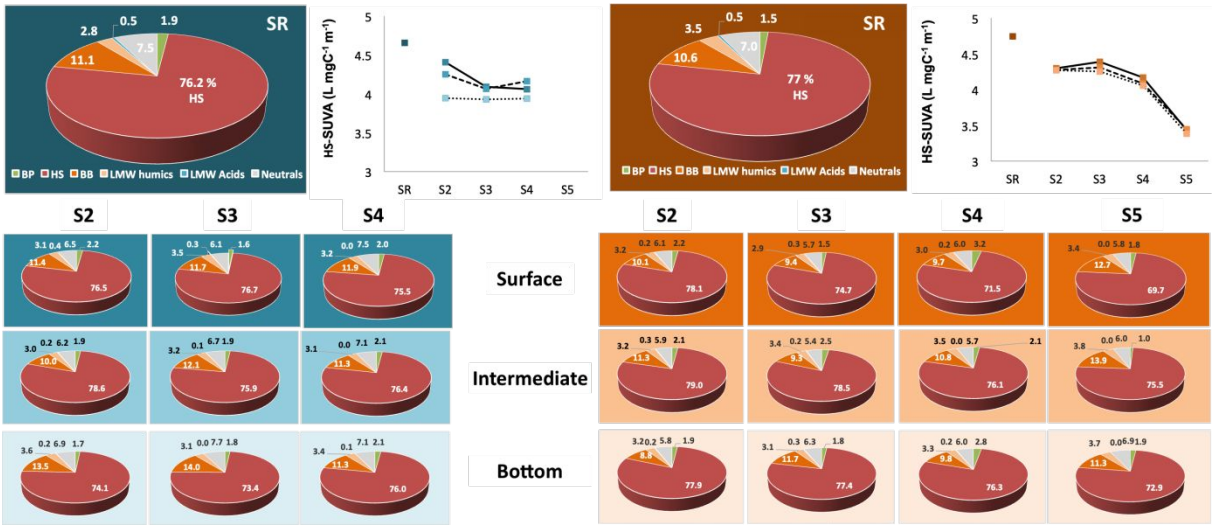

Figure 3. Hydrophilic DOM composition obtained by LC–OCD for water sampled under ice-covered (blue) and ice-free (orange) conditions. The SUVA values of LC-separated humic like substances (Humic SUVA) for all sampling sites are represented near the DOM composition of Shuya River. BP: Biopolymers; HS: humic; BB: buiding blocks; LMW: low molecular weight components.

215

216 **Effect of Shuya River dispersion in the bay on HS molecular mass characteristics**

217 The humic fractions were further characterized by determining number-averaged molecular
218 mass M_n, weight-averaged molecular mass M_w and polydispersity parameter D (M_w over M_n
219 ratios) (**Table S2**).

220 The molecular mass characteristics obtained for SR and Petrozavodsk Bay corresponded to
221 the M_n of fulvic acid extracts with a relatively higher aromaticity but associated to high M_w
222 resulting in a high polydispersity.[57] These results strongly support that humic components are
223 in a highly agglomerated state in line with the high HIX values. The average molecular
224 masses and polydispersity of the HS in the river were generally higher in March than those
225 obtained in June. This can be related to differences in the composition of the HS components,
226 in the temperature of the river (0.2 °C in March vs 9.2 °C in June) as well as in conductivity
227 (40.6 µS cm^{-1} in March vs 27.4 µS cm^{-1} in June), given that their aromatic properties which

could lead to different degrees of agglomeration were identical (HS-SUVA, SR, **Figure 3**). The differences in the runoff composition can be due to differences in precipitations, permafrost and snow-melting, and changes in soil horizons involved as DOM sources that are drained.[34, 41]

For both seasons, these parameters tended to decrease throughout the bay with some exceptions (grey shades in **Table S2**). Under ice-covered conditions, the M_w of HS, and to some extended the M_n, decreased with the distance of river mouth in the two shallowest depths of the bay. This phenomenon was accompanied by a more pronounced decrease of D, suggesting a decrease in the HS agglomeration and the loss of higher molecular mass HS while the river reached the bay. In addition, all the parameters were relatively homogenous on a site-by-site comparison in the shallowest depths. This can be due to the vertical mixing of the riverine HS with the surface layer since a vertical convective flux with a vertical velocity of 5 mm s^{-1} was measured at the site S3, and was shown to take place until 11.5−19.5 m depth.[36] At the bottom layer of the bay, the obtained low M_w, agreed with low SUVA and a higher contribution of BB for the two first sampling sites, and the highest M_n were also measured at this locations, while at the site S4 all the measurements agreed with an increase in the HS agglomeration state, and lower M_n were measured. As it was shown that an accumulation of dissolved inorganic carbon due to sediments respiration occurred at the bottom of the bay,[38] a diffusion from the sediments of more recalcitrant HS (biodegraded) with lower aromatic character and but higher molecular mass could contribute to the DOM. Overall, M_w values showed an excellent correlation with the HS-SUVA values (r^2 = 0.93), whereas no significant correlation was found for M_n values (r^2 = 0.13). These results imply that the decrease in aromaticity of the HS components is correlated to the decrease in the proportion of higher molecular mass components.

Under ice-free conditions, higher molecular masses were found in the bay samples as compared with SR, but with a decrease in the agglomeration state of the riverine HS probably linked to the higher conductivity in the bay (47.7−48.8 μS cm^{-1} from sites S2 to S4). The dynamic changes in size of HS components are influenced by several environmental factors such as the ionic strength or pH leading to the formation of large supramolecular architectures (> 1 μm).[58] It could be assumed that the HS components with high aromaticity were removed from the water column leading in this case to an apparent decrease in the agglomeration state of remaining HS. For the first two sampling locations in the bay, the M_w were comparable but decreased in the last sampling location. Overall, a decrease in the number-average molecular mass was measured throughout the bay in the two shallowest layers. Despite of the apparent increase in all the parameters measured at the site S2 in the bottom layer, a clear positive correlation between the M_w and D values with HS−SUVA (r^2 = 0.85 and r^2 = 0.86 respectively) was obtained for the overall samples of the ice-free period, but like it was observed for the ice-covered period the M_n values were poorly related to this variable (r^2 < 0.1). In the lake, even if the conductivity was higher than that in the bay (55.5 μS cm^{-1}), our results are consistent with a lower agglomeration state of the HS components. Considering the limited water exchanges between the bay and the lake due to the presence of the thermal bar,[59] and that the sampling point in the lake was located at 40 km from the site S4, the humic components of the lake were certainly not directly from the river origin, explaining why they have slightly higher M_n values.

A global decrease in molecular masses (M_p) and the hydrodynamic diameters (d_{hp}) of the chromophoric HS, that were obtained at the peak maximum by AF4−DAD (light orange signals in **Figure 4**), was observed in both March and June while the river entered the bay and were even smaller in the lake samples (**Table S3**). Although correlations between the two different techniques are difficult to be drawn directly because of the different detectors,

277 carriers or data treatments that were used,[60] the M_p value obtained corroborated qualitatively
278 with the loss of aromatic character of HS (HS−SUVA; $r^2 = 0.5$) together with molecular
279 characteristics quantified by LC−OCD (D, $r^2 = 0.6$; M_w, $r^2 = 0.5$) except with M_n ($r^2 < 0.1$).
280 Overall, our findings suggested that the decrease in DOC concentrations was associated to a
281 decrease in proportions of HS components with higher molecular mass/size and aromaticity
282 leading to a decrease in agglomeration state the HS originated from the SR through the bay
283 before they could reach the lake.
284
285 **Influence of the bay hydrochemistry on the stability of the colloidal pool**
286 Considering the high iron and aluminum concentrations characterizing the studied site (**Table**
287 **S4**) and the interplay that could exist between HS and mineral oxides for their role in metal
288 dispersion, the distribution of metal bound to both HS and mineral oxides colloids were
289 determined for several metals by AF4−ICPMS (**Figure S3**). Their preferential association to
290 the colloidal components of different size is given in the **SI**. Results obtained for Fe, Cu, Al
291 and Pb from the river to the lake gradient are illustrated in **Figure 4**.
292 The Cu fractograms clearly followed DOM UV-signals of the HS, without the implication of
293 small dissolved molecules that should co-elute at the beginning of the size-fractionation.
294 Hence, Cu was considered to bind exclusively to these colloids. The Al, Pb and Fe elemental
295 distributions were shifted to higher sizes than UV-signal corresponding to the HS. Similar
296 shifts of metal distributions were previously reported,[44, 61] and suggest a molecular mass/size
297 dependency of metal binding to HS. The interactions of these elements with small-iron oxide
298 clusters (SCIox) overlapping the HS size distributions could also account for such size
299 increase.[7, 8] Hence, the quantification of M−HS was done by taking into account the
300 contribution of these components by a signal deconvolution.[45]

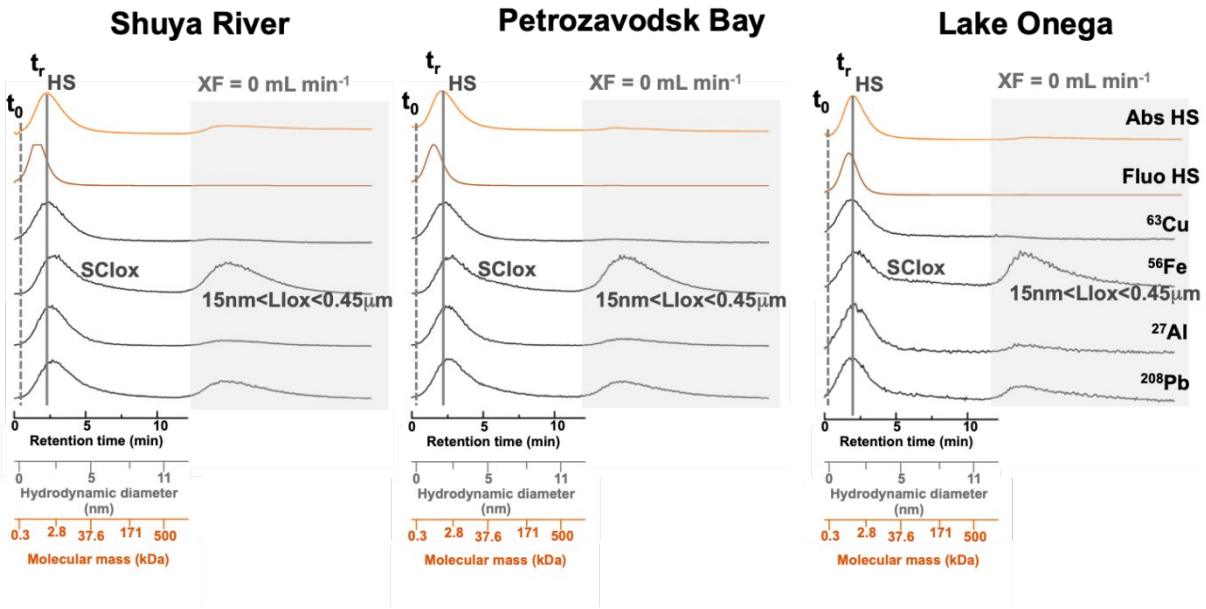

Figure 4. Association of Cu, Fe, Al and Pb with colloidal pool (> 300 Da) obtained by AF4−DAD−FluoD−ICPMS for water sampled under ice-free conditions at river mouth (Shuya River), site S3 (Petrozavodsk Bay) and Lake Onega. The dashed lines indicate the void time (t_o) corresponding to the beginning of sample elution; The plain lines indicate the retention time of the peak maximum of absorbance at λ = 254 nm signal, corresponding to HS chromophoric components. Corresponding molecular masse (M_p) and hydrodynamic diameters (d_{hp}) for all samples are given in **Table S3**. Under these conditions, colloids (HS and SCIox) with hydrodynamic size bellow corresponding to M_p = 1000 kDa are separated. XF = 0 mL min^{-1} corresponds to the time after the switch-off of the cross-flow, where the large colloids co-elute simultaneously (LIox). The raw AF4–ICPMS fractograms for all the samples are presented in the **SI**.

The evolutions of the distribution in the colloidal pool (M–HS, (M–)SCIox and (M–)LIox, as defined in **Figure 4**) originated from SR throughout the bay to the lake are given in the **Figure S4**. Despite the different seasonal regimes in the river watershed, the colloidal content (recovery) was relatively stable but the metallic distributions between the three components were slightly altered in SR. In agreement with its high affinity for the HS and the relatively constant dissolved Cu concentrations in all the samples (**Table S4**), the colloidal copper (Cu–HS) remained at high level in both seasons (**Figure S4 A, B**). By contrast, the colloidal proportions and contents of Fe, Al and Pb (**Figure S4 C–H**) dropped rapidly in the bay under ice-coved conditions and were more affected by the bay hydrochemistry as compared with ice-free conditions. These results can be explained by the higher river discharge in June than

312 in March and the difference of stratification, leading to differences in dilution and mixing of
313 the river water with the bay water. In addition, we found larger proportions of LIox (60−80%)
314 in the samples from March as compared with those from June (50−60%), where sizeable
315 proportion of Fe was also present as SCIox, 25−30% (**Figure S5 A, B**). The lowest
316 proportions of LIox were found at the surface of sites S2 and S3 in March, and the lowest Fe
317 colloidal recoveries (i.e. colloidal proportion in the dissolved phase) were obtained for these
318 two samples (31% of total dissolved Fe).
319 The percentages of M−HS were larger for Al and Pb with Al−HS contributing to 35−60% and
320 50% of the colloidal Al in March and June respectively (**Figure S5 C, D**) and Pb−HS
321 contributing to 30−40% and 30% of the colloidal Pb in March and June respectively (**Figure**
322 **S5 E, F**). The lowest M−LIox proportions and colloidal recoveries for these two elements
323 were found at the upper layer of sites S2 and S3 when the bay was ice-covered. The lower
324 colloidal quantities measured just under-ice could rely on exposure of colloids to light at the
325 vicinity of ice-cover that could alter the structure of iron-oxides together with humic
326 substances. Indeed both the production of LMW components and the increased coagulation of
327 iron-oxides due to sunlight have been identified for similar humic-rich waters.[62] Photo-
328 alteration of HS have been reported to alter metal complexation properties and their
329 aromaticity.[27, 44] No clear changes in the proportions of HS, their SUVA (**Figure 3**) or size
330 parameters (**Table S2, S3**) were however observable if compared with those obtained at the
331 intermediary depth for the sites where the recovery of iron was higher (54% and 62% for sites
332 S2 and S3, respectively). This strongly suggests that the formation of larger colloids rather
333 than changes in the quality of DOM may be responsible for the colloidal depletion obtained at
334 sites S2 and S3. A recent study also revealed that freeze-thawing of iron and DOC rich waters
335 lead to mineral colloids coagulation.[63] Such effect on colloidal stability at the water-ice

interface is unexplored but can also explain the results for the metals that are part-off or bound-to iron-oxides colloids.

Overall, except for the under-ice layer, the distribution of metal within the colloidal pool was relatively stable in the bay, suggesting that they dispersed in a conservative manner.

Dispersion of M−HS through the river-bay-lake continuum and changes in metal binding capacity

The dispersion of M−HS is shown in **Figure 5**. For Cu a progressive decrease throughout the river-lake gradient in June was observed (**Figure 5 B**) while in March, the Cu−HS content followed similar winter stratification pattern as DOC and other associated parameters (**Figure 5 A**). To relate how the changes in the quality of the riverine HS can affect their metal binding capacity, the ratios Cu−HS/Cu−HS_{SR} obtained by AF4-ICPMS were related to the carbon contents of HS (C−HS/C−HS_{SR}) obtained by LC-OCD. A good 1:1 correlation (slope = 1.17; r^2 = 0.92) was found between all the Cu−HS/Cu−HS_{SR} and C−HS/C−HS_{SR} independently of the sampling seasons **(Figure 5 C)**. This strongly suggested that HS components able to bind Cu were not affected by the decrease of SUVA and certainly do not participate to the changes in the agglomeration state of HS we previously observed. In addition, this correlation is ameliorated if the values obtained for the lake (slope = 0.97; r^2 = 0.92), indicative of the different metal binding properties of the lacustrine HS.

Similar dispersion profiles were obtained for Fe−HS with higher drops while reaching the bay in both March and June (by 60% and 40%, at intermediary depth, **Figure 5 D, E**). The relationship between SR-normalized Fe−HS and C−HS was exponential (**Figure 5 F**), and a decrease in Fe binding capacity of the HS throughout the bay to the lake was observed (**Figure S6 A**). The decrease in the proportion of the more aromatic HS components by removal from the water column could be suggested as a reason for such loss of Fe binding

capacity. This mechanism can be supported by the high concentration of dissolved Fe measured at the bottom layer of the site S2 (**Table S4**), at least under ice-free conditions (**Table 1**).

Similarly to Fe−HS, a rapid decrease in both Al−HS and Pb−HS was observed along the upper layers of the river-bay gradient in March (**Figure 5 G, J**), but a progressive increase was observed along the bottom of the bay. This highlights that in the deepest layer, the Al−HS and Pb−HS do not necessarily follow the trend observed for Cu−HS and suggests that the microbial respiration and higher temperatures could be responsible for the diffusion of Pb and Al (together with Fe) from the sediments to the bottom layer (**Table S4**).

Under ice-free conditions, Al−HS decreased rapidly (by 40%) while reaching the bay and further diminished following the dilution gradient from the bay to the lake, without any horizontal stratification but was found at low level in the lake (**Figure 4 K**). Similarly to Fe, the dissolved concentration of Al was found to be higher at the bottom layer than in the water column at site S2 suggesting its removal at the entry of the bay (**Table S4**). Even though a linear relationship is observed between Al−HS/Al−HS_{SR} and C−HS/C−HS_{SR}, it is characterized by a slope above the unity (slope = 1.34; r^2 = 0.96, **Figure 4 I**). This suggested that the Al binding capacity of the HS components decreased (**Figure S6 B**) as their size and aromaticity decreased.

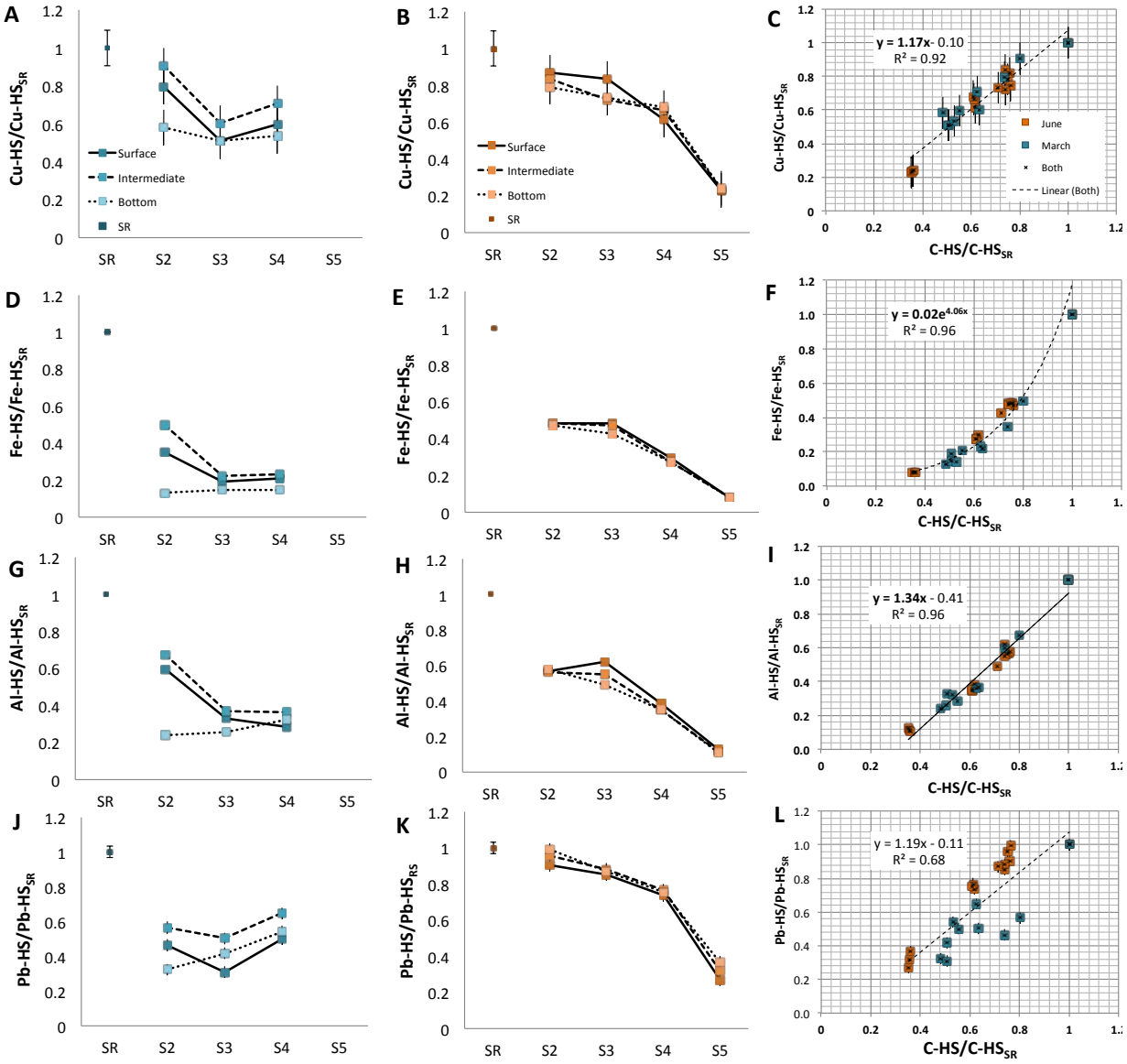

Figure 5. Dispersion of metal bound to humic fraction (M−HS) in the river–bay–lake Onega continuum under ice-cover (blue) and ice-free conditions (orange). Values obtained by AF4−ICPMS by direct integration for Cu−HS **(A, B)** or using 3 components deconvolution of the Fe **(D, E)**, Al **(G, H)** and Pb **(J, K)** signals were normalized to those obtained for Shuya River (M−HS/M−HS_{SR}). The correlation between M−HS ratios *versus* normalized to Shuya River humic substances concentration measured by LC−OCD (C−HS/C−HS_{SR}) are presented on the left-side (**C, F, I, L**). Error bars are represented if larger than the symbol size.

380

381

382 In the case of humic bound Pb, no good relationship between the two measurements was

383 found (**Figure 4 L**). When the bay was ice-covered, the lowest Pb−HS were found in the

384 upper layer of site S2 site S3 (**Figure 4 L**), suggesting that major changes in water chemistry

385 linked to the colloidal pump at the vicinity of the ice-cover may change the colloidal
386 speciation of Pb at these locations. Since this element can interact with HS *via* a ternary
387 complex involving Fe,[10, 22, 64] the changes affecting Fe−HS residence in the water column
388 certainly altered the binding of Pb. In addition, the values of Pb−HS under ice-free conditions
389 were higher than expected based on the C−HS measurements. Similarly to the dissolved
390 concentrations of Fe and Al, those of Pb are characterized by a strong drop in the bay (**Table**
391 **S4**). This suggested that an input of colloidal material (rather than dissolve Pb) from other
392 sources than SR, such as atmospheric deposition or as snow-melting around the bay,[65] may
393 have contributed to the high concentrations of Pb−HS we observed. This is also in agreement
394 with the elevate contents in colloidal Pb measured in the bay as compared to SR inputs in
395 June (**Figure S4**).
396 The presence of two main types of HS components differing by their ability to form
397 aggregates by supramolecular interactions (colloidal behavior) have been demonstrated.[66, 67] It
398 can be suggested that the HS components able to bind Fe, Al and Pb may have a colloidal
399 behavior and others, that bound Cu in addition, have a macromolecular behavior explaining
400 their relative stability in the water column. Further studies are needed to validate such a kind
401 of molecular specificity in metal binding among HS components.
402
403 **Environmental Implications**
404 In river catchments containing high iron and DOC concentrations, the variations of the
405 molecular mass together with the aromatic character of HS have been already reported.[9, 68] In
406 addition, the preferential molecular binding to iron or aluminum (hydr)oxides was shown to
407 increase the removal HS components with high aromatic and hydrophobic characters together
408 with mineral colloids.[69] These changes in HS properties have been shown to occur at the
409 confluence of rivers with variable pH and sources. The relative conservative proportions in

410 the colloidal pool while the river diluted in the bay suggests a poor interplay between HS and
411 iron-oxides colloids and considering the relatively constant and neutral pH of the studied
412 samples (6.8−7.2), we proposed that observed changes we reported in the apparent size of HS
413 are related to a decrease in the proportion of HS components that have high molecular mass,
414 aromaticity and binding capacity for Al and Fe through the bay.
415 Although controlling the dispersion of HS in the bay, the seasonal changes in the bay hydro-
416 physical characteristics and the differences in the river discharge do not alter the phenomenon
417 we observed. Both the ice-cover and the occurrence of a thermal-bar were previously reported
418 to delay the dispersion of the riverine inputs from the bay into the Lake Onego, and to
419 decrease the rate of water exchange in the bay to 2.9 month in winter.[35] But considering the
420 relatively conservative composition of the organic matter we observed upon dilution in the
421 bay, the mixing with lacustrine HS can also account to the change in apparent size
422 distribution[70] and further the changes in binding properties we reported. Further studies are
423 needed to define which parameters (e.g. conductivity, dilution, light) have controlled or were
424 responsible of this phenomenon.
425
426 **Supporting Information**
427 Sampling site locations and main characteristics of the bay hydrochemistry under ice-covered
428 and ice-free conditions. Details regarding experimental procedures for fluorescence analysis
429 of DOM, LC-OCD, AF4-ICPMS. EEM and AF4-ICPMS fractograms acquired for all the
430 samples. Tables containing molecular mass parameters and hydrodynamic diameter obtained
431 by LC-OCD or AF4-DAD and total metal concentration of metals obtained by ICPMS. The
432 figures the colloidal distribution of metal and binding capacity. The following file is available
433 free of charge in one file (PDF)
434

AUTHOR INFORMATION

Corresponding Author

*Isabelle A.M. Worms

tel: + 41 22 379 05 90

e-mail: isabelle.worms@unige.ch

*Vera I. Slaveykova

Tel: +41 22 379 03 35

e-mail **:** vera.slaveykova@unige.ch

Isabelle A.M. Worms ORCID: https://orcid.org/0000-0002-7498-0078

Vera I. Slaveykova ORCID: http://orcid.org/0000-0002-8361-2509

Natacha Tofield-Pasche ORCID: https://orcid.org/0000-0002-9578-9301

ACKNOWLEDGEMENTS

We acknowledged Mariapaola Ambrosone, Teofana Chonova for water sampling and Quentin Ramel and Killian Kavanagh for fluorescence measurements. Warm thanks are addressed to the three reviewers involved. Their critical comments have more than improve the quality of the present document. The work was supported by the International Project “Lake Ladoga: life under ice – interplay of under-ice processes by global change” and Swiss National Science Foundation grant 200021_166089.

REFERENCES

1. Wilkinson, K. J.; Lead, J. R., *Environmental Colloids and Particles. Behaviour, Separation and Characterisation*. John Wiley Sons, Ltd. Chichester, UK: 2007; Vol. 10.
2. Baalousha, M.; Kammer, F. V. D.; Motelica-Heino, M.; Baborowski, M.; Hofmeister, C.; Le Coustumer, P., Size-based speciation of natural colloidal particles by flow field flow fractionation, inductively coupled plasma-mass spectroscopy, and transmission electron microscopy/X-ray energy dispersive spectroscopy: Colloids-trace element interaction. *Environ. Sci. Technol.* **2006,** *40*, (7), 2156-2162.
3. Lyvén, B.; Hassellöv, M.; Turner, D. R.; Haraldsson, C.; Andersson, K., Competition between iron- and carbon-based colloidal carriers for trace metals in a freshwater assessed using flow field-flow fractionation coupled to ICPMS. *Geochimica et Cosmochimica Acta* **2003,** *67*, (20), 3791-3802.
4. Stolpe, B.; Hassellov, M., Changes in size distribution of fresh water nanoscale colloidal matter and associated elements on mixing with seawater. *Geochimica Et Cosmochimica Acta* **2007,** *71*, (13), 3292-3301.
5. Stolpe, B.; Hassellov, M.; Andersson, K.; Turner, D. R., High resolution ICPMS as an on-line detector for flow field-flow fractionation; multi-element determination of colloidal size distributions in a natural water sample. *Analytica Chimica Acta* **2005,** *535*, (1-2), 109-121.
6. Worms, I. A. M.; Al-Gorani Szigeti, Z.; Dubascoux, S.; Lespes, G.; Traber, J.; Sigg, L.; Slaveykova, V. I., Colloidal organic matter from wastewater treatment plant effluents: Characterization and role in metal distribution. *Water Research* **2010,** *44*, (1), 340-350.
7. Neubauer, E.; Schenkeveld, W. D. C.; Plathe, K. L.; Rentenberger, C.; von der Kammer, F.; Kraemer, S. M.; Hofmann, T., The influence of pH on iron speciation in podzol extracts: Iron complexes with natural organic matter, and iron mineral nanoparticles. *Science of The Total Environment* **2013,** *461-462*, 108-116.
8. Cuss, C. W.; Grant-Weaver, I.; Shotyk, W., AF4-ICPMS with the 300 Da Membrane To Resolve Metal-Bearing "Colloids" < 1 kDa: Optimization, Fractogram Deconvolution, and Advanced Quality Control. *Analytical Chemistry* **2017,** *89*, (15), 8027-8035.
9. Neubauer, E.; Köhler, S. J.; von der Kammer, F.; Laudon, H.; Hofmann, T., Effect of pH and Stream Order on Iron and Arsenic Speciation in Boreal Catchments. *Environ. Sci. Technol.* **2013,** *47*, (13), 7120-7128.
10. Cuss, C. W.; Donner, M. W.; Grant-Weaver, I.; Noernberg, T.; Pelletier, R.; Sinnatamby, R. N.; Shotyk, W., Measuring the distribution of trace elements amongst dissolved colloidal species as a fingerprint for the contribution of tributaries to large boreal rivers. *Science of The Total Environment* **2018,** *642*, 1242-1251.
11. Lapworth, D. J.; Stolpe, B.; Williams, P. J.; Gooddy, D. C.; Lead, J. R., Characterization of Suboxic Groundwater Colloids Using a Multi-method Approach. *Environ. Sci. Technol.* **2013,** *47*, (6), 2554-2561.
12. Liao, P.; Li, W.; Jiang, Y.; Wu, J.; Yuan, S.; Fortner, J. D.; Giammar, D. E., Formation, Aggregation, and Deposition Dynamics of NOM-Iron Colloids at Anoxic–Oxic Interfaces. *Environ. Sci. Technol.* **2017,** *51*, (21), 12235-12245.
13. Busch, V. M.; Loosli, F.; Santagapita, P. R.; Buera, M. P.; Stoll, S., Formation of complexes between hematite nanoparticles and a non-conventional galactomannan gum. Toward a better understanding on interaction processes. *Science of The Total Environment* **2015,** *532*, 556-563.

14. Palomino, D.; Stoll, S., Fulvic acids concentration and pH influence on the stability of hematite nanoparticles in aquatic systems. *Journal of Nanoparticle Research* **2013,** *15*, (2), 1428.
15. Philippe, A.; Schaumann, G. E., Interactions of Dissolved Organic Matter with Natural and Engineered Inorganic Colloids: A Review. *Environ. Sci. Technol.* **2014,** *48*, (16), 8946-8962.
16. Pokrovsky, O. S.; Shirokova, L. S.; Zabelina, S. A.; Vorobieva, T. Y.; Moreva, O. Y.; Klimov, S. I.; Chupakov, A. V.; Shorina, N. V.; Kokryatskaya, N. M.; Audry, S.; Viers, J.; Zoutien, C.; Freydier, R., Size Fractionation of Trace Elements in a Seasonally Stratified Boreal Lake: Control of Organic Matter and Iron Colloids. *Aquatic Geochemistry* **2012,** *18*, (2), 115-139.
17. Pokrovsky, O. S.; Manasypov, R. M.; Loiko, S. V.; Krickov, I. A.; Kopysov, S. G.; Kolesnichenko, L. G.; Vorobyev, S. N.; Kirpotin, S. N., Trace element transport in western Siberian rivers across a permafrost gradient. *Biogeosciences* **2016,** *13*, (6), 1877-1900.
18. Shirokova, L. S.; Pokrovsky, O. S.; Moreva, O. Y.; Chupakov, A. V.; Zabelina, S. A.; Klimov, S. I.; Shorina, N. V.; Vorobieva, T. Y., Decrease of concentration and colloidal fraction of organic carbon and trace elements in response to the anomalously hot summer 2010 in a humic boreal lake. *Science of the Total Environment* **2013,** *463*, 78-90.
19. Pokrovsky, O. S.; Shirokova, L. S., Diurnal variations of dissolved and colloidal organic carbon and trace metals in a boreal lake during summer bloom. *Water Research* **2013,** *47*, (2), 922-932.
20. Xu, H. C.; Yang, C. M.; Jiang, H. L., Aggregation kinetics of inorganic colloids in eutrophic shallow lakes: Influence of cyanobacterial extracellular polymeric substances and electrolyte cations. *Water Research* **2016,** *106*, 344-351.
21. Xu, H. C.; Xu, M. W.; Li, Y. N.; Liu, X.; Guo, L. D.; Jiang, H. L., Characterization, origin and aggregation behavior of colloids in eutrophic shallow lake. *Water Research* **2018,** *142*, 176-186.
22. Pedrot, M.; Dia, A.; Davranche, M.; Bouhnik-Le Coz, M.; Henin, O.; Gruau, G., Insights into colloid-mediated trace element release at the soil/water interface. *J Colloid Interface Sci* **2008,** *325*, (1), 187-97.
23. Ren, J.; Packman, A. I., Coupled stream-subsurface exchange of colloidal hematite and dissolved zinc, copper, and phosphate. *Environ Sci Technol* **2005,** *39*, (17), 6387-94.
24. Schafer, T.; Artinger, R.; Dardenne, K.; Bauer, A.; Schuessler, W.; Kim, J. I., Colloid-borne americium migration in Gorleben groundwater: significance of iron secondary phase transformation. *Environ Sci Technol* **2003,** *37*, (8), 1528-34.
25. Weng, L.; Fest, E. P.; Fillius, J.; Temminghoff, E. J.; van Riemsdijk, W. H., Transport of humic and fulvic acids in relation to metal mobility in a copper-contaminated acid sandy soil. *Environ Sci Technol* **2002,** *36*, (8), 1699-704.
26. Tercier Waeber, M., Stoll, S., & Slaveykova, V. , Trace metal behavior in surface waters: Emphasis on dynamic speciation, sorption processes and bioavailability. *Archives Des Sciences* **2012,** *65*, 119-142.
27. Worms, I. A. M.; Slaveykova, V. I.; Wilkinson, K. J., Lead Bioavailability to Freshwater Microalgae in the Presence of Dissolved Organic Matter: Contrasting Effect of Model Humic Substances and Marsh Water Fractions Obtained by Ultrafiltration. *Aquatic Geochemistry* **2015,** *21*, (2-4), 217-230.
28. Denfeld, B. A.; Baulch, H. M.; del Giorgio, P. A.; Hampton, S. E.; Karlsson, J., A synthesis of carbon dioxide and methane dynamics during the ice-covered period of northern lakes. *Limnology and Oceanography Letters* **2018,** *3*, (3), 117-131.

29. Stolpe, B.; Zhou, Z.; Guo, L.; Shiller, A. M., Colloidal size distribution of humic- and protein-like fluorescent organic matter in the northern Gulf of Mexico. *Marine Chemistry* **2014,** *164*, 25-37.
30. Zhou, Z.; Stolpe, B.; Guo, L.; Shiller, A. M., Colloidal size spectra, composition and estuarine mixing behavior of DOM in river and estuarine waters of the northern Gulf of Mexico. *Geochimica et Cosmochimica Acta* **2016,** *181*, 1-17.
31. Xu, H.; Houghton, E. M.; Houghton, C. J.; Guo, L., Variations in size and composition of colloidal organic matter in a negative freshwater estuary. *Science of The Total Environment* **2018,** *615*, 931-941.
32. Sabylina, A. V.; Lozovik, P. A.; Zobkov, M. B., Water chemistry in Onega Lake and its tributaries. *Water Resources* **2010,** *37*, (6), 842-853.
33. Filatov, N. N.; Viruchalkina, T. Y.; Dianskiy, N. A.; Nazarova, L. E.; Sinukovich, V. N., Intrasecular variability in the level of the largest lakes of Russia. *Doklady Earth Sciences* **2016,** *467*, (2), 393-397.
34. Filatov, N.; Baklagin, V.; Efremova, T.; Nazarova, L.; Palshin, N., Climate change impacts on the watersheds of Lakes Onego and Ladoga from remote sensing and in situ data. *Inland Waters* **2019,** *9*, (2), 130-141.
35. Lozovik, P. A.; Zobkov, M. B.; Borodulina, G. S.; Tokarev, I. V., Assessing External Water Exchange of Lake Bays by Water Chemistry Characteristics. *Water Resources* **2019,** *46*, (1), 94-102.
36. Bogdanov, S.; Zdorovennova, G.; Volkov, S.; Zdorovennov, R.; Palshin, N.; Efremova, T.; Terzhevik, A.; Bouffard, D., Structure and dynamics of convective mixing in Lake Onego under ice-covered conditions. *Inland Waters* **2019,** *9*, (2), 177-192.
37. Efremova, T. A.; Sabylina, A. V.; Lozovik, P. A.; Slaveykova, V. I.; Zobkova, M. V.; Pasche, N., Seasonal and spatial variation in hydrochemical parameters of Lake Onego (Russia): insights from 2016 field monitoring. *Inland Waters* **2019,** *9*, (2), 227-238.
38. Pasche, N.; Hofmann, H.; Bouffard, D.; Schubert, C. J.; Lozovik, P. A.; Sobek, S., Implications of river intrusion and convective mixing on the spatial and temporal variability of under-ice CO2. *Inland Waters* **2019,** *9*, (2), 162-176.
39. Suarez, E. L.; Tiffay, M.-C.; Kalinkina, N.; Tchekryzheva, T.; Sharov, A.; Tekanova, E.; Syarki, M.; Zdorovennov, R. E.; Makarova, E.; Mantzouki, E.; Venail, P.; Ibelings, B. W., Diurnal variation in the convection-driven vertical distribution of phytoplankton under ice and after ice-off in large Lake Onego (Russia). *Inland Waters* **2019,** *9*, (2), 193-204.
40. Wüest, A.; Pasche, N.; Ibelings, B. W.; Sharma, S.; Filatov, N., Life under ice in Lake Onego (Russia) – an interdisciplinary winter limnology study. *Inland Waters* **2019,** *9*, (2), 125-129.
41. Chmiel, H. E.; Hofmann, H.; Sobek, S.; Efremova, T.; Pasche, N., Where does the river end? Drivers of spatiotemporal variability in CO2 distribution and flux in the inflow area of a large boreal lake. *Limnology and Oceanography* **accepted**.
42. Bouffard, D.; Zdorovennov, R. E.; Zdorovennova, G. E.; Pasche, N.; Wuest, A.; Terzhevik, A. Y., Ice-covered Lake Onega: effects of radiation on convection and internal waves. *Hydrobiologia* **2016,** *780*, (1), 21-36.
43. Huber, S. A.; Balz, A.; Abert, M.; Pronk, W., Characterisation of aquatic humic and non-humic matter with size-exclusion chromatography – organic carbon detection – organic nitrogen detection (LC-OCD-OND). *Water Research* **2011,** *45*, (2), 879-885.
44. Worms, I. A. M.; Adenmatten, D.; Miéville, P.; Traber, J.; Slaveykova, V. I., Photo-transformation of pedogenic humic acid and consequences for Cd(II), Cu(II) and Pb(II) speciation and bioavailability to green microalga. *Chemosphere* **2015,** *138*, 908-915.

45. Dublet, G.; Worms, I.; Frutschi, M.; Brown, A.; Zünd, G. C.; Bartova, B.; Slaveykova, V. I.; Bernier-Latmani, R., Colloidal Size and Redox State of Uranium Species in the Porewater of a Pristine Mountain Wetland. *Environ. Sci. Technol.* **2019**.
46. Pokrovsky, O. S.; Schott, J., Iron colloids/organic matter associated transport of major and trace elements in small boreal rivers and their estuaries (NW Russia). *Chemical Geology* **2002,** *190*, (1-4), 141-179.
47. Chen, H.; Zheng, B.; Song, Y.; Qin, Y., Correlation between molecular absorption spectral slope ratios and fluorescence humification indices in characterizing CDOM. *Aquatic Sciences* **2011,** *73*, (1), 103-112.
48. Weishaar, J. L.; Aiken, G. R.; Bergamaschi, B. A.; Fram, M. S.; Fujii, R.; Mopper, K., Evaluation of Specific Ultraviolet Absorbance as an Indicator of the Chemical Composition and Reactivity of Dissolved Organic Carbon. *Environ. Sci. Technol.* **2003,** *37*, (20), 4702-4708.
49. Coble, P. G., Characterization of marine and terrestrial DOM in seawater using excitation-emission matrix spectroscopy. *Marine Chemistry* **1996,** *51*, (4), 325-346.
50. Huguet, A.; Vacher, L.; Relexans, S.; Saubusse, S.; Froidefond, J. M.; Parlanti, E., Properties of fluorescent dissolved organic matter in the Gironde Estuary. *Organic Geochemistry* **2009,** *40*, (6), 706-719.
51. McKnight, D. M.; Boyer, E. W.; Westerhoff, P. K.; Doran, P. T.; Kulbe, T.; Andersen, D. T., Spectrofluorometric characterization of dissolved organic matter for indication of precursor organic material and aromaticity. *Limnology and Oceanography* **2001,** *46*, (1), 38-48.
52. Zsolnay, A.; Baigar, E.; Jimenez, M.; Steinweg, B.; Saccomandi, F., Differentiating with fluorescence spectroscopy the sources of dissolved organic matter in soils subjected to drying. *Chemosphere* **1999,** *38*, (1), 45-50.
53. Lozovik, P. A.; Morozov, A. K.; Zobkov, M. B.; Dukhovicheva, T. A.; Osipova, L. A., Allochthonous and autochthonous organic matter in surface waters in Karelia. *Water Resources* **2007,** *34*, (2), 204-216.
54. Ohno, T., Fluorescence Inner-Filtering Correction for Determining the Humification Index of Dissolved Organic Matter. *Environ. Sci. Technol.* **2002,** *36*, (4), 742-746.
55. Hansen, A. M.; Kraus, T. E. C.; Pellerin, B. A.; Fleck, J. A.; Downing, B. D.; Bergamaschi, B. A., Optical properties of dissolved organic matter (DOM): Effects of biological and photolytic degradation. *Limnology and Oceanography* **2016,** *61*, (3), 1015-1032.
56. Sutton, R.; Sposito, G., Molecular structure in soil humic substances: The new view. *Environmental Science & Technology* **2005,** *39*, (23), 9009-9015.
57. Chin, Y. P.; Aiken, G.; Oloughlin, E., MOLECULAR-WEIGHT, POLYDISPERSITY, AND SPECTROSCOPIC PROPERTIES OF AQUATIC HUMIC SUBSTANCES. *Environmental Science & Technology* **1994,** *28*, (11), 1853-1858.
58. Baalousha, M.; Motelica-Heino, M.; Le Coustumer, P., Conformation and size of humic substances: Effects of major cation concentration and type, pH, salinity, and residence time. *Colloids and Surfaces a-Physicochemical and Engineering Aspects* **2006,** *272*, (1-2), 48-55.
59. Auer, M. T.; Gatzke, T. L., The spring runoff event, thermal bar formation, and cross margin transport in Lake Superior. *Journal of Great Lakes Research* **2004,** *30*, 64-81.
60. Her, N.; Amy, G.; Foss, D.; Cho, J. W., Variations of molecular weight estimation by HP-size exclusion chromatography with UVA versus online DOC detection. *Environ. Sci. Technol.* **2002,** *36*, (15), 3393-3399.
61. Bolea, E.; Gorriz, M. P.; Bouby, M.; Laborda, F.; Castillo, J. R.; Geckeis, H., Multielement characterization of metal-humic substances complexation by size exclusion

655 chromatography, asymmetrical flow field-flow fractionation, ultrafiltration and inductively
656 coupled plasma-mass spectrometry detection: A comparative approach. *Journal of*
657 *Chromatography A* **2006,** *1129*, (2), 236-246.
658 62. Oleinikova, O. V.; Drozdova, O. Y.; Lapitskiy, S. A.; Demin, V. V.; Bychkov, A. Y.;
659 Pokrovsky, O. S., Dissolved organic matter degradation by sunlight coagulates organo-
660 mineral colloids and produces low-molecular weight fraction of metals in boreal humic
661 waters. *Geochimica et Cosmochimica Acta* **2017,** *211*, 97-114.
662 63. Pokrovsky, O. S.; Karlsson, J.; Giesler, R., Freeze-thaw cycles of Arctic thaw ponds
663 remove colloidal metals and generate low-molecular-weight organic matter. *Biogeochemistry*
664 **2018,** *137*, (3), 321-336.
665 64. Neubauer, E.; von der Kammer, F. D.; Hofmann, T., Using FLOWFFF and HPSEC to
666 determine trace metal colloid associations in wetland runoff. *Water Research* **2013,** *47*, (8),
667 2757-2769.
668 65. Javed, M. B.; Cuss, C. W.; Grant-Weaver, I.; Shotyk, W., Size-resolved Pb
669 distribution in the Athabasca River shows snowmelt in the bituminous sands region an
670 insignificant source of dissolved Pb. *Scientific Reports* **2017,** *7*, 43622.
671 66. Baigorri, R.; Fuentes, M.; Gonzalez-Gaitano, G.; Garcia-Mina, J. M., Analysis of
672 molecular aggregation in humic substances in solution. *Colloids and Surfaces a-*
673 *Physicochemical and Engineering Aspects* **2007,** *302*, (1-3), 301-306.
674 67. Baigorri, R.; Fuentes, M.; Gonzalez-Gaitano, G.; Garcia-Mina, J. M., Simultaneous
675 presence of diverse molecular patterns in humic substances in solution. *Journal of Physical*
676 *Chemistry B* **2007,** *111*, (35), 10577-10582.
677 68. Benedetti, M.; Ranville, J. F.; Ponthieu, M.; Pinheiro, J. P., Field-flow fractionation
678 characterization and binding properties of particulate and colloidal organic matter from the
679 Rio Amazon and Rio Negro. *Organic Geochemistry* **2002,** *33*, (3), 269-279.
680 69. McKnight, D. M.; Bencala, K. E.; Zellweger, G. W.; Aiken, G. R.; Feder, G. L.;
681 Thorn, K. A., Sorption of dissolved organic carbon by hydrous aluminum and iron oxides
682 occurring at the confluence of Deer Creek with the Snake River, Summit County, Colorado.
683 *Environ. Sci. Technol.* **1992,** *26*, (7), 1388-1396.
684 70. Dulaquais, G.; Breitenstein, J.; Waeles, M.; Marsac, R.; Riso, R., Measuring dissolved
685 organic matter in estuarine and marine waters: size-exclusion chromatography with various
686 detection methods. *Environmental Chemistry* **2018,** *15*, (7), 436-449.
687

Supporting Information

Dissolved Organic Matter and Associated Trace Metal Dynamics from River to Lake, Under Ice-covered and Ice-free Conditions

Isabelle A. M. Worms[1], Hannah E. Chmiel[2], Jacqueline Traber[3], Natacha Tofield-Pasche[2] and Vera I. Slaveykova[1*]*

[1]Environmental Biogeochemistry and Ecotoxicology, Department F.-A. Forel for environmental and aquatic sciences, Earth and Environmental Sciences, Faculty of Sciences, University of Geneva, 66, boulevard Carl-Vogt, CH-1211 Geneva, Switzerland

[2] Limnological Center, Ecole Polytechnique Fédérale de Lausanne (EPFL), Station 2, 1015 Lausanne, Switzerland

[3] Process Engineering, Eawag, Überlandstrasse 133, 8600 Dübendorf, Switzerland

*corresponding authors

tel: + 41 22 379 05 90; +41 22 379 03 35

e-mail: isabelle.worms@unige.ch; vera.slaveykova@unige.ch

Number of Pages: 21
1 Supplementary Material, 3 Sections, 6 Figures, 4 Tables

Table of contents

List of Figures

List of Tables

Section 1: Lake Onega, sampling sites and main characteristics of the Bay hydrochemistry under ice-covered and ice-free conditions

Table S1. Abbreviation list of the sampling sites, location according to Figure S1, coordinates and sampling depths for March and June 2017 campaigns.

Station	Name and Location	Coordinates	Sampling depth (m)
March 2017			
SR	Shuya River	N61 50.830 E34 21.454	0.5
S2	Site 2 Petrozavodsk Bay	N61 49.613 E34 22.195	0.5, 15.5, 21
S3	Site 3 Petrozavodsk Bay	N61 48.826 E34 25.600	0.5, 18.5, 27.5
S4	Site 4 Petrozavodsk Bay	N61 46.707 E34 31.797	1, 18.5, 30
June 2017			
SR	Shuya River	N61 50.830 E34 21.454	1
S2	Site 2 Petrozavodsk Bay	N61 49.600 E34 22.258	1, 10, 21
S3	Site 3 Petrozavodsk Bay	N61 48.447 E34 26.018	1, 19, 25
S4	Site 4 Petrozavodsk Bay	N61 46.707 E34 31.797	1, 10, 30
S5	Site 5 Lake Onega	N61 41.937 E34 58.995	1, 20, 40

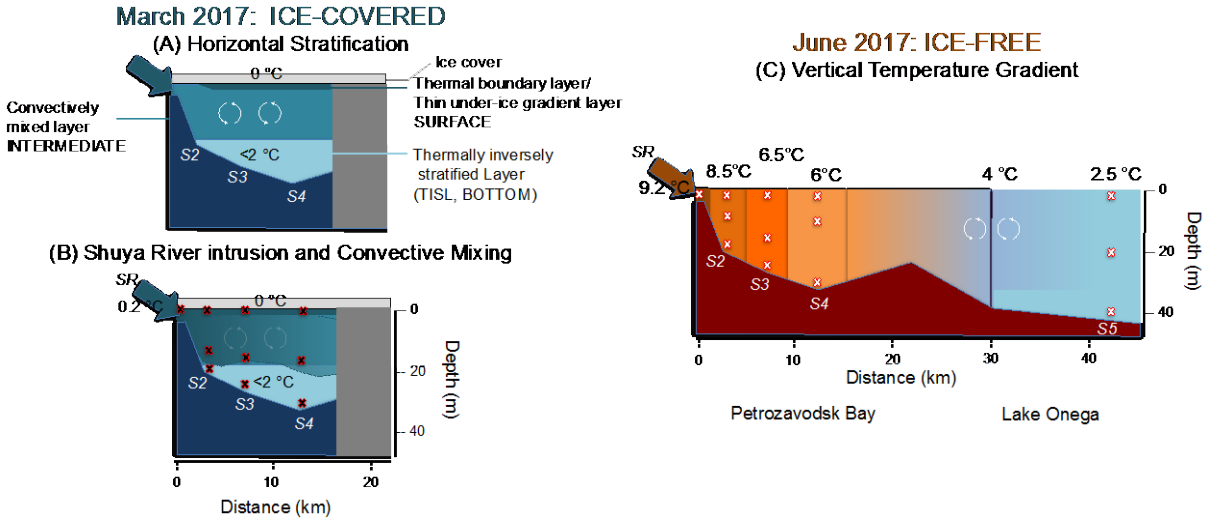

Figure S1. Main limnological characteristics of the Bay under ice-covered (March, A, B) and ice-free conditions (June, C). Crosses indicate the depths of sampling for each sites. The figure is described in the main text and further in SI.

Two main figures can be retained for winter limnological behaviors of the Bay. As previously described [S1], the Bay is horizontally stratified in winter, with under-ice convection promoted by higher temperature at the bottom and the influence of radiation on the snow-free ice-cover with the formation of a thin thermal boundary layer. This type of behavior has been identified in Petrozavodsk Bay in March 2015 [S2] (**Fig. S1A**). However, this convectively driven mixing is predominant solely when Shuya River inflow is low as compared to high discharge leading to river intrusion in the Bay (**Fig. S1B**). Both phenomena as been addressed in the Petrozavodsk Bay recently for March 2015 and 2016.[S3] In March 2017, the discharged was high enough for the river intrusion to occur as well.[S4] This has great influences on CO_2 and CH_4 inputs in this mixing zone during winter[S3, 4] and further on gazes atmospheric fluxes after ice-off.[S4] Lake ice-melt leads to a seasonal transition to summer stratification of the lake, as it was the case for Lake Onega in June 2015 and 2016. In June 2017 (**Fig. S1C**), the summer stratification was not established and a vertical temperature gradient due to the confluence of warm river inflow and cold lake water occurred in the Petrozadovosk Bay.

Such is characterized by the presence of a thermal bar at 4°C (maximum water density)[S5] that separate vertically the lake from the inputs of the river, the lake staying under winter inverted stratification.[S4]

Section 2: Details regarding experimental procedures

S2.1 Characterization of fluorogenic DOM

The excitation-emission matrices (EEMs) were used to characterize DOM fluorogenic constituents (e.g. humic-like or protein-like fluorophores).[S6] Fluorescence spectra were recorded on an LS 55 Luminescence Spectrometer (Perkin-Elmer) using a 3 mL, 1 cm path length quartz cuvette. EEMs were generated by recording emission spectra from 300 to 550 nm at 0.5 nm steps for excitation wavelengths between 200 and 450 nm with 5 nm steps. The fluorescence index (FIX),[S7] which provides information about the extent of condensation of humic substances, and thus their origin, was derived from EEM fingerprints according to: FIX = (I_{500}/I_{450}) for λ_{Ex} = 370 nm. The biological index (BIX), DOM freshness, was estimated from the ratio between fluorescence intensity at λ_{Em} =380 nm *vs* λ_{Em} = 430 nm (BIX = I_{380}/I_{430}) for λ_{Ex} = 310 nm as previously detailed.[S8] The humification index (HIX), linked to condensation degree of humic substances, was determined as the ratio of emission spectrum areas between λ_{Em} 435–480 nm over the emission spectrum areas between λ_{Em} 435–480 nm plus λ_{Em} 300–345 nm (HIX= $I_{435-480}$ / ($I_{435-480}$ + $I_{330-345}$) at λ_{Ex} = 254 nm.[S9] Obtained values for BIX, HIX and FIX for a 10 mg L^{-1} Suwannee River fulvic acid (SRFA, IHSS) gave expected values for pedogenic HS isolated from riverine DOM: 0.32, 0.96 and 1.15 for BIX, HIX, and FIX respectively. Specific UV absorbance (SUVA) at 254 nm[S10] was determined by LC-OCD, by dividing the ratio of the SAC to the respective carbon content[S11] and corrected for potential iron interferences. [S12]

S2.2 DOM changes in composition using LC-OCD

The organic matter constituents were characterized by size exclusion chromatography coupled in-line to a fixed wavelength detector flashing at 254nm (UVD), an organic carbon and nitrogen detector (Liquid chromatography - organic carbon detection, LC-OCD-OND (DOC-Labor Dr. Huber, Germany). The gel filtration column Toyopearl® HW-50S (Tosoh Bioscience) with a fractionation range of 20 to 0.1 kDa was used. The detection limit had been previously determined to be 10 µg C L^{-1} for the OCD.[S13] Depending on their total organic contents, the samples were diluted 5 times before measurements and 2 mL injection volumes for the chromatograms were used. Samples were eluted at 1 mL min^{-1} using a 24 mM phosphate buffer at pH = 6.6. DOC was further differenced in hydrophilic (HydDOC) that are separated in the column and hydrophobic DOC (HoDOC) that could not be eluted. Corresponding HydDOM components were further classified in biopolymers (BP), humic substances (HS), building blocks (BB), low molecular weight humic (LMWH), acids (LMWA) and neutral (LMWN) compounds according to their retention times and UV absorbance properties. Molecular mass distribution of the humic fraction in the samples were obtained from deconvolution of LC-OCD chromatograms using a Poisson binomal distribution shape, calibrated with SRFA (M_n = 0.796 kDa) and SRHA (M_n = 1.108 kDa) from whom molecular mass weight (M_w) and molecular mass number (M_n) average were obtained together with the polydispersity parameter ($D = M_w / M_n$).[S11] The aromaticity of the HS fraction, which may be expressed as the ratio of SAC to carbon, plotted against the molecular weight as M_n defines the origin of the humic substances. The higher the aromaticity (SUVA) and molecularity (M_n) of HS, the older the water, respectively the less impact of environment, human or agriculture may be expected.[S11, 14, 15] The derivation of SUVA by LC-OCD combining separation of samples based on the size and hydrophobicity

parameters for chromogenic DOM was found to be free of iron-oxides interferences as no differences in their values were found after corrective equation[S12] and this despite quite high values of total iron (**Table S4**) we found in the samples.

S2.3 Method for size separation of the small colloidal pool

An AF2000 Focus (Postnova Analytics; Landsberg, Germany) was coupled to diode array and fluorescence detectors, (DAD, FLD, Postnova Analytics, Landsberg, Germany), on-line with ICPMS (model 7700x, Agilent technologies, Morges, Switzerland). A membrane with a low molecular weight cut-off (Polyestersulfone, 0.3 kDa) and high cross-flow (2.7 mL min^{-1}) were used for fractionation, and 10 mM NH_4NO_3 pH = 7 was used as eluent. The molecular mass (M_p) and hydrodynamic diameter (d_h) measured for the Shuya River by AF4-DAD were in the same order as those found for Standard Suwannee River Fulvic Acid (SRFA, M_p = 1.7 kDa and d_{hp} = 1.6 nm). The M_p values in our studies were higher than those found for Suwannee River NOM isolate, and three different boreal river samples with M_p of 0.970 kDa using the same type of instrument.[S16] This difference can be attributed to difference in separation conditions, such as: mobile phase ionic strength or pH, cross-flow programs, calibration of the channel, deconvolution of peaks or to analyte-specific properties such as the initial agglomeration state of the HS components and their origin.[S17, 18]

Section 3: Additional figures, tables and information for main text discussion

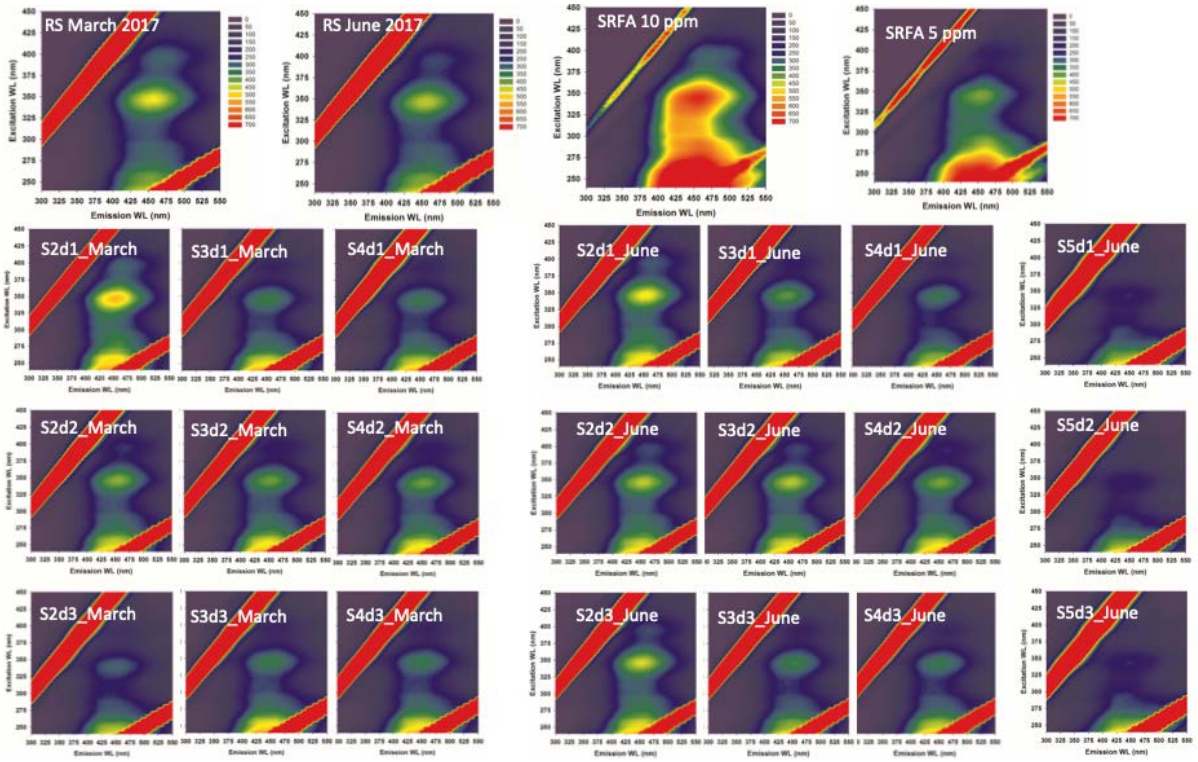

Figure S2. Excitation-Emission Matrix (EEM) of all the samples and SRFA under the same fluorescence measurement conditions. d1, d2, and d3 referred to sampling depths respectively Surface, Intermediary and Bottom.

Table S2. Molecular mass characteristics of the humic components obtained by LC-OCD

		ice-covered				
		SR	**S2**	**S3**	**S4**	**S5**
Surface	M_n (Da)	758	709	606	657	
	M_w (Da)	4090	3407	2630	2726	
	D	**5.39**	**4.81**	**4.34**	**4.15**	
Intermediate	M_n (Da)		607	622	651	
	M_w (Da)		3285	2898	2891	
	D		**5.41**	**4.66**	**4.44**	
Bottom	M_n (Da)		726	736	605	
	M_w (Da)		2644	2649	2654	
	D		**3.64**	**3.6**	**4.39**	

		ice-free				
		SR	**S2**	**S3**	**S4**	**S5**
Surface	M_n (Da)	613	673	658	600	638
	M_w (Da)	3088	3173	3137	2658	2087
	D	**5.04**	**4.71**	**4.77**	**4.43**	**3.27**
Intermediate	M_n (Da)		688	651	636	673
	M_w (Da)		3174	3077	2866	2260
	D		**4.61**	**4.73**	**4.51**	**3.36**
Bottom	M_n (Da)		590	719	615	557
	M_w (Da)		3071	3188	2719	2055
	D		**5.21**	**4.43**	**4.42**	**3.69**

M_n: number average molecular mass, M_w: weight average molecular mass; D: polydispersity parameter (M_w / M_n).

Table S3. Molecular mass and hydrodynamic diameters of the chromophoric humic components obtained by AF4-DAD

		ice-covered				
		SR	**S2**	**S3**	**S4**	**S5**
Surface	M_p (Da)	2028	1790	1790	1641	
	d_{hp} (nm)	1.7	1.6	1.6	1.5	
Intermediate	M_p (Da)		1790	1790	1531	
	d_{hp} (nm)		1.6	1.6	1.5	
Bottom	M_p (Da)		977	977	1670	
	d_{hp} (nm)		1.2	1.2	1.5	

		ice-free				
		SR	**S2**	**S3**	**S4**	**S5**
Surface	M_p (Da)	2143	1699	1641	1302	1164
	d_{hp} (nm)	1.7	1.6	1.5	1.4	1.3
Intermediate	M_p (Da)		1641	1531	1326	1164
	d_{hp} (nm)		1.5	1.5	1.4	1.3
Bottom	M_p (Da)		1451	1670	997	1164
	d_{hp} (nm)		1.5	1.6	1.2	1.3

M_p: molecular mass and d_{ph}: hydrodynamic diameter at maximum peak of absorbance recorded at λ =254 nm by DAD (see **Figure 4**) were determined using polyestersulfonate standards for external calibration, or AF4 elution theory employing BSA as standard respectively.[S19, 20]

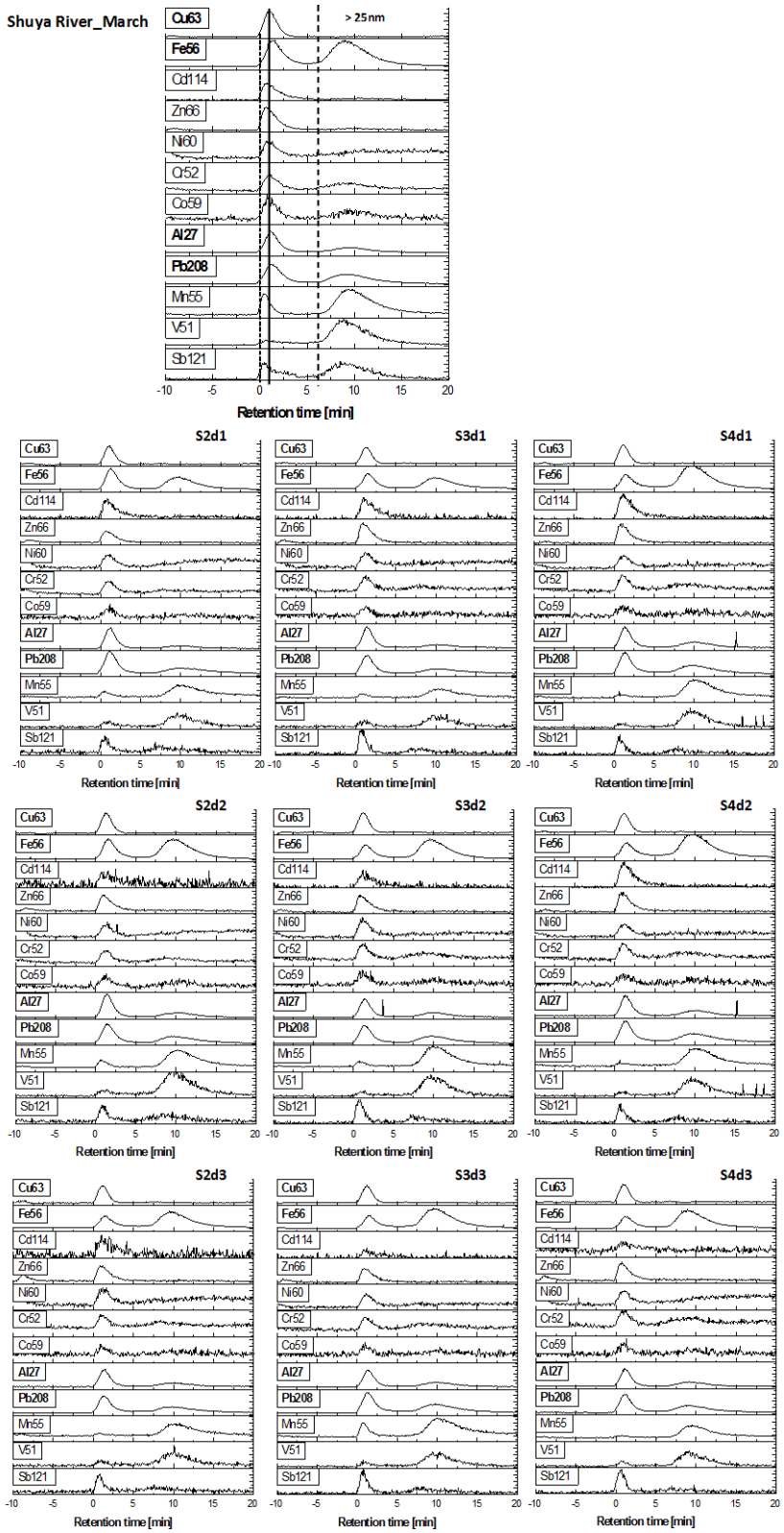

Figure S3. Raw elemental fractograms obtained by AF4-ICPMS for the samples obtained during the ice-cover campaign

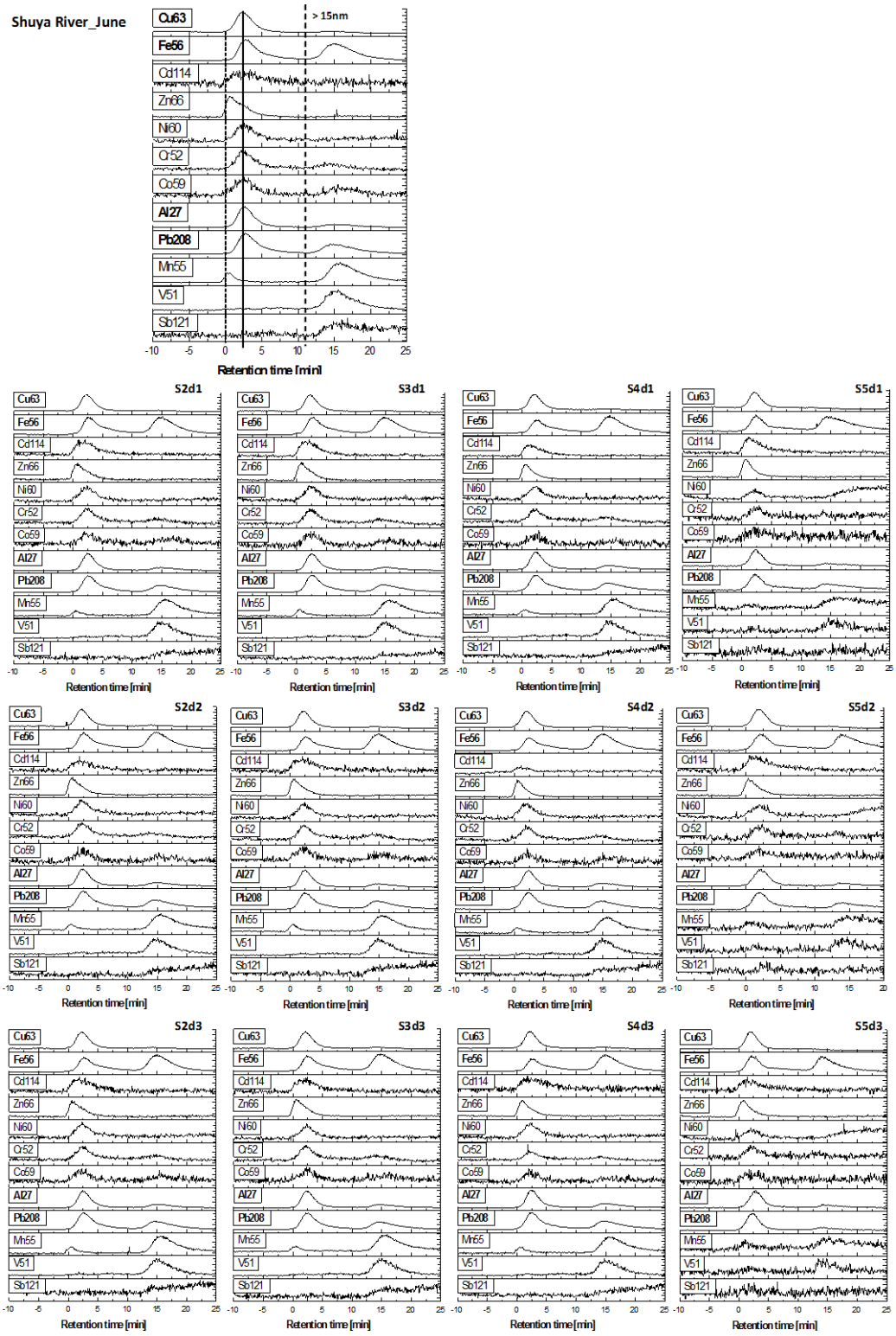

Figure S3 (count). Figure S3. Raw elemental fractograms obtained by AF4-ICPMS for the samples obtained during the ice-free campaign

Supplementary informations concerning preferential binding of trace metals in the colloidal pool.

The colloidal distribution of the metals depends on their intrinsic reactivity [S21-23] and can be grouped in our system as follows: (i) metals bound to small dissolved molecules (void, dashed lines in the **Figure S3**), and humics (HS, the elution time at peak of maximum intensity is indicated as plain line, **Figure S3**): Zn and Cd; (ii) metals bound mainly to the HS: Cu, Ni; (iii) metals bound to both humic components and large mineral colloids: Co, Cr, Al, Pb or Fe (in order of increasing association with larger colloids), and (iv) associated to or part-off large mineral colloids: Mn, V and Sb. The high Fe signal combined with low absorbance at 254 nm and fluorescence in the large colloidal pool strongly suggested the presence of iron-(hydr)-oxides, with d_h > 15-25 nm in the studied waters (LIox).

For all the samples we analyze, the distribution of Cu and Ni traced the absorbance signal at 254 nm corresponding to humic substances. The Co and Cr signals were low and noisy, but their major fractions followed a similar pattern, with binding to humic substances and slight influences of iron-oxides colloids, which is consistent with the literature results for this two metals obtained with ultrafiltration.[S24] For Co, Cr, Cu and Ni, the present results are also consistent with the existing AF4 studies showing the preferential association of these metals with HS, while the elution of Pb in the larger size fraction was related to the presence of iron-oxide of small size in Alaskan rivers.[S25] While often found as truly dissolved material or as alumino-silicates,[S16] Al was found associated to HS in the Shuya River colloids. Alumino-silicates were not present in waters in of the Karelian region and Al was previously found to associate mainly with iron-oxide colloids of M_w > 10 kDa or with colloids of size between 1−10 kDa and below.[S24] The size distribution of Al also depended on DOC concentration using cascade ultrafiltration for Al species < 0.2 μm.[S26] Large manganese colloids were also

likely present as Mn-oxy-hydroxides, since neither organic matter nor iron were demonstrated previously to have influence on its size distribution in rivers from this region in previous study.[S24] Both V and Sb oxyanions are found exclusively associated with LIox, contrasting with the behavior of Cr. For V our results are in agreement with those found by ultrafiltration but Sb was previously found to be mainly associated to DOM < 10 kDa in organic-rich rivers from this region.[S24] Our results for Sb also contrasted with those of a recent study showing that it did not correspond with the behavior of DOM or Fe.[S26] However the detection of Sb bound to the smaller colloidal fraction could be limited by the AF4−ICPMS method itself, because a maximum 30 % of all Sb is expected to be bound to the whole colloidal pool.[S26]

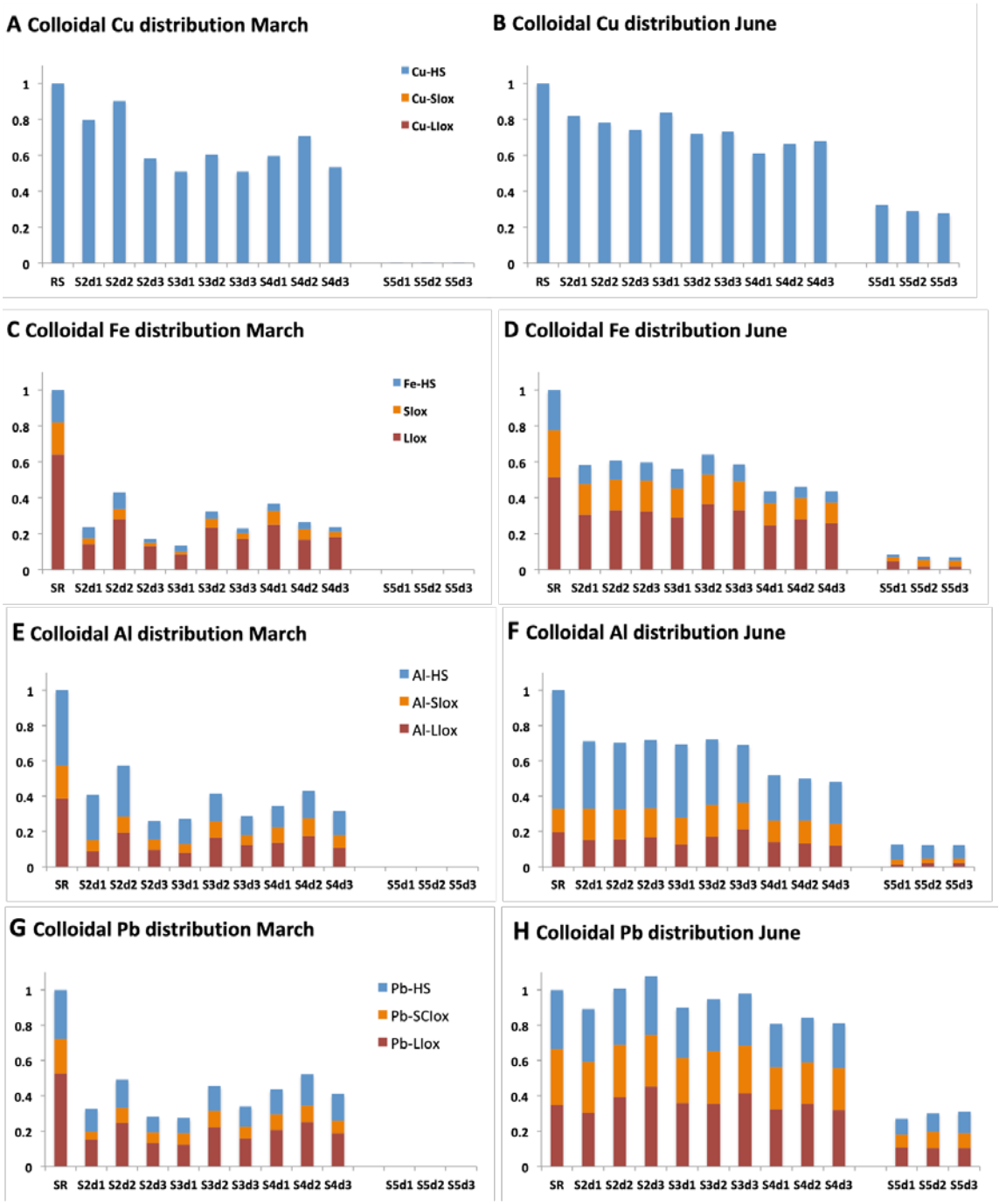

Figure S4. Dispersion of the metallic colloidal distribution in the river–bay–lake Onega continuum for the two sampling campaigns for Cu (A, B), Fe (C, D), Al (E, F) and Pb (G, H).

Values obtained by peaks deconvolution of the ICPMS fractograms using 3 components: metal bound to the humic components (M−HS, blue) metal bound to small iron-oxide clusters (M−SCIox, orange) and metal bound to large iron-oxides colloids (M−LIox, red). Measurements were normalized to the total colloidal content obtained in the Shuya river for each element. d1, d2, and d3 referred to sampling depths respectively Surface, Intermediary and Bottom.

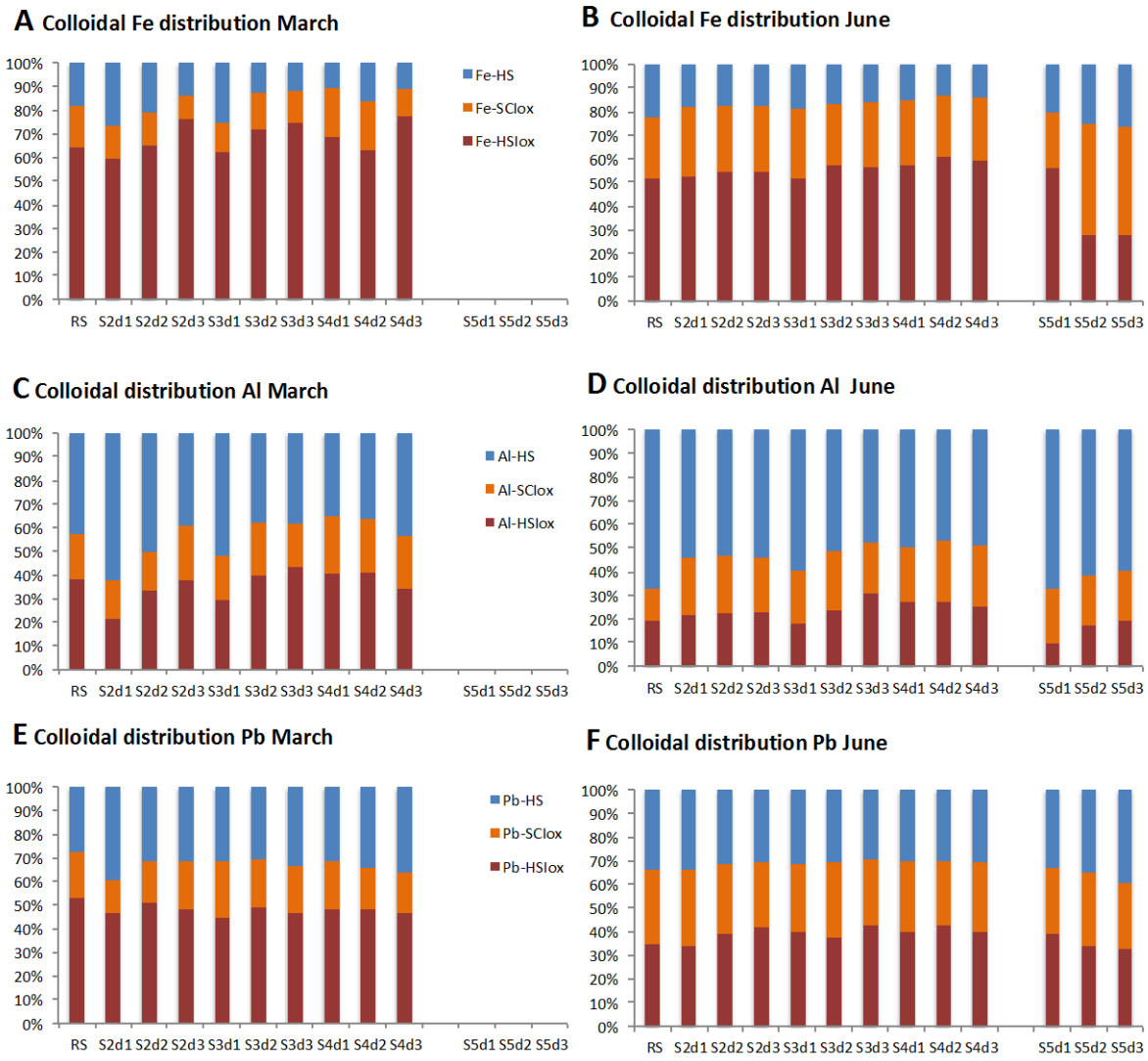

Figure S5. Three components colloidal distribution for Fe (A, B) ; Al (D,E) and Pb (F,G) obtained by ICPMS fractograms deconvolution of the HS peak. d1, d2, and d3 referred to sampling depths respectively Surface, Intermediary and Bottom.

Table S4. Total concentrations of dissolved Fe, Al, Cu and Pb measured by ICPMS

		Ice-covered				
		SR	**S2**	**S3**	**S4**	**S5**
Fe (ppb)	**d1**	**786** (33)	**453** (20)	**252** (10)	**248** (14)	
	d2		**464** (16)	**306** (15)	**326** (12)	
	d3		**178** (7)	**201** (7)	**248** (11)	
Al (ppb)	**d1**	**109** (4)	**72** (4)	**45** (2)	**46** (2)	
	d2		**75** (3)	**55** (2)	**58** (2)	
	d3		**33** (2)	**38** (2)	**50** (7)	
Cu (ppb)	**d1**	**3.2** (0.1)	**1.58** (0.07)	**1.48** (0.08)	**1.43** (0.17)	
	d2		**0.91** (0.05)	**1.26** (0.36)	**1.37** (0.07)	
	d3		**1.05** (0.08)	**1.01** (0.11)	**1.14** (0.06)	
Pb (ppb)	**d1**	**0.45** (0.02)	**0.34** (0.03)	**0.25** (0.00)	**0.16** (0.00)	
	d2		**0.27** (0.01)	**0.18** (0.01)	**0.19** (0.00)	
	d3		**0.14** (0.01)	**0.13** (0.01)	**0.16** (0.04)	

		Ice-free				
		SR	**S2**	**S3**	**S4**	**S5**
Fe (ppb)	**d1**	**647** (31)	**272** (1)	**370** (1)	**289** (10)	**29** (1)
	d2		**303** (4)	**387** (9)	**287** (3)	**28** (1)
	d3		**404** (20)	**327** (11)	**268** (4)	**32** (1)
Al (ppb)	**d1**	**142** (9)	**87** (1)	**91** (1)	**67** (2)	**10** (1)
	d2		**85** (1)	**91** (0)	**66** (1)	**11** (0)
	d3		**97** (3)	**77** (2)	**63** (1)	**10** (0)
Cu (ppb)	**d1**	**3** (2)	**3.99** (0.01)	**3.59** (-)	**3.10** (0.14)	**3.21** (0.13)
	d2		**2.66** (0.05)	**2.14** (0.41)	**2.19** (0.06)	**1.80** (0.01)
	d3		**2.84** (0.58)	**2.31** (0.10)	**1.76** (0.57)	**1.67** (0.05)
Pb (ppb)	**d1**	**0.78** (0.34)	**0.36** (0.02)	**0.38** (0.01)	**0.47** (0.01)	**0.24** (0.04)
	d2		**0.35** (0.00)	**0.40** (0.09)	**0.31** (0.00)	**0.21** (0.06)
	d3		**0.78** (0.14)	**0.28** (0.02)	**0.24** (0.03)	**0.20** (0.05)

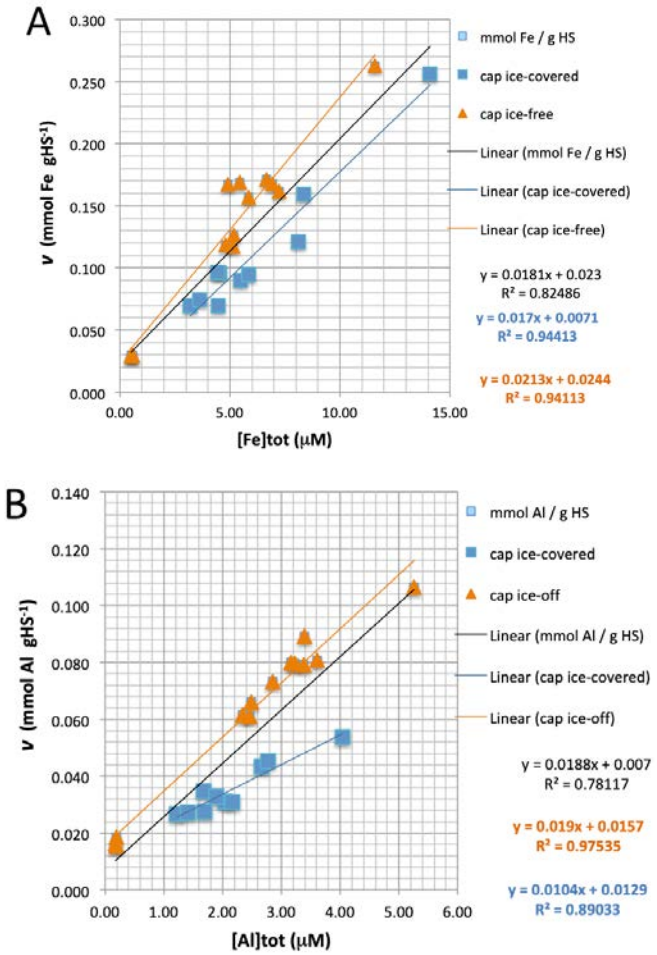

Figure S6. Fe (A) and Al (B) binding capacities as the function of total dissolved metals.

References

S1. Kirillin, G.; Leppäranta, M.; Terzhevik, A.; Granin, N.; Bernhardt, J.; Engelhardt, C.; Efremova, T.; Golosov, S.; Palshin, N.; Sherstyankin, P.; Zdorovennova, G.; Zdorovennov, R., Physics of seasonally ice-covered lakes: a review. *Aquatic Sciences* **2012,** *74*, (4), 659-682.

S2. Bouffard, D.; Zdorovennov, R. E.; Zdorovennova, G. E.; Pasche, N.; Wuest, A.; Terzhevik, A. Y., Ice-covered Lake Onega: effects of radiation on convection and internal waves. *Hydrobiologia* **2016,** *780*, (1), 21-36.

S3. Pasche, N.; Hofmann, H.; Bouffard, D.; Schubert, C. J.; Lozovik, P. A.; Sobek, S., Implications of river intrusion and convective mixing on the spatial and temporal variability of under-ice CO2. *Inland Waters* **2019,** *9*, (2), 162-176.

S4. Chmiel, H. E.; Hofmann, H.; Sobek, S.; Efremova, T.; Pasche, N., Where does the river end? Drivers of spatiotemporal variability in CO2 distribution and flux in the inflow area of a large boreal lake.
Limnology and Oceanography, **accepted**.

S5. Holland, P. R.; Kay, A., A review of the physics and ecological implications of the thermal bar circulation. *Limnologica* **2003,** *33*, (3), 153-162.

S6. Worms, I. A. M.; Slaveykova, V. I.; Wilkinson, K. J., Lead Bioavailability to Freshwater Microalgae in the Presence of Dissolved Organic Matter: Contrasting Effect of Model Humic Substances and Marsh Water Fractions Obtained by Ultrafiltration. *Aquatic Geochemistry* **2015,** *21*, (2-4), 217-230.

S7. McKnight, D. M.; Boyer, E. W.; Westerhoff, P. K.; Doran, P. T.; Kulbe, T.; Andersen, D. T., Spectrofluorometric characterization of dissolved organic matter for indication of precursor organic material and aromaticity. *Limnology and Oceanography* **2001,** *46*, (1), 38-48.

S8. Huguet, A.; Vacher, L.; Relexans, S.; Saubusse, S.; Froidefond, J. M.; Parlanti, E., Properties of fluorescent dissolved organic matter in the Gironde Estuary. *Organic Geochemistry* **2009,** *40*, (6), 706-719.

S9. Zsolnay, A.; Baigar, E.; Jimenez, M.; Steinweg, B.; Saccomandi, F., Differentiating with fluorescence spectroscopy the sources of dissolved organic matter in soils subjected to drying. *Chemosphere* **1999,** *38*, (1), 45-50.

S10. Weishaar, J. L.; Aiken, G. R.; Bergamaschi, B. A.; Fram, M. S.; Fujii, R.; Mopper, K., Evaluation of Specific Ultraviolet Absorbance as an Indicator of the Chemical Composition and Reactivity of Dissolved Organic Carbon. *Environ. Sci. Technol.* **2003,** *37*, (20), 4702-4708.

S11. Huber, S. A.; Balz, A.; Abert, M.; Pronk, W., Characterisation of aquatic humic and non-humic matter with size-exclusion chromatography – organic carbon detection – organic nitrogen detection (LC-OCD-OND). *Water Research* **2011,** *45*, (2), 879-885.

S12. Poulin, B. A.; Ryan, J. N.; Aiken, G. R., Effects of Iron on Optical Properties of Dissolved Organic Matter. *Environ. Sci. Technol.* **2014,** *48*, (17), 10098-10106.

S13. Huber, S. A.; Frimmel, F. H., Flow injection analysis for organic and inorganic carbon in the low-ppb range. *Analytical Chemistry* **1991,** *63*, (19), 2122-2130.

S14. Stewart, T. J.; Traber, J.; Kroll, A.; Behra, R.; Sigg, L., Characterization of extracellular polymeric substances (EPS) from periphyton using liquid chromatography-

organic carbon detection–organic nitrogen detection (LC-OCD-OND). *Environmental Science and Pollution Research* **2013,** *20*, (5), 3214-3223.
S15. Velten, S.; Knappe, D. R. U.; Traber, J.; Kaiser, H.-P.; von Gunten, U.; Boller, M.; Meylan, S., Characterization of natural organic matter adsorption in granular activated carbon adsorbers. *Water Research* **2011,** *45*, (13), 3951-3959.
S16. Cuss, C. W.; Grant-Weaver, I.; Shotyk, W., AF4-ICPMS with the 300 Da Membrane To Resolve Metal-Bearing "Colloids" < 1 kDa: Optimization, Fractogram Deconvolution, and Advanced Quality Control. *Analytical Chemistry* **2017,** *89*, (15), 8027-8035.
S17. Cuss, C. W.; Guéguen, C., Determination of relative molecular weights of fluorescent components in dissolved organic matter using asymmetrical flow field-flow fractionation and parallel factor analysis. *Analytica Chimica Acta* **2012,** *733*, 98-102.
S18. Cuss, C. W.; Guéguen, C., Distinguishing dissolved organic matter at its origin: Size and optical properties of leaf-litter leachates. *Chemosphere* **2013,** *92*, (11), 1483-1489.
S19. Worms, I. A. M.; Adenmatten, D.; Miéville, P.; Traber, J.; Slaveykova, V. I., Photo-transformation of pedogenic humic acid and consequences for Cd(II), Cu(II) and Pb(II) speciation and bioavailability to green microalga. *Chemosphere* **2015,** *138*, 908-915.
S20. Worms, I. A. M.; Al-Gorani Szigeti, Z.; Dubascoux, S.; Lespes, G.; Traber, J.; Sigg, L.; Slaveykova, V. I., Colloidal organic matter from wastewater treatment plant effluents: Characterization and role in metal distribution. *Water Research* **2010,** *44*, (1), 340-350.
S21. Wilkinson, K. J.; Lead, J. R., *Environmental Colloids and Particles. Behaviour, Separation and Characterisation*. John Wiley Sons, Ltd. Chichester, UK: 2007; Vol. 10.
S22. Tercier Waeber, M., Stoll, S., & Slaveykova, V. , Trace metal behavior in surface waters: Emphasis on dynamic speciation, sorption processes and bioavailability. *Archives Des Sciences* **2012,** *65*, 119-142.
S23. Lyvén, B.; Hassellöv, M.; Turner, D. R.; Haraldsson, C.; Andersson, K., Competition between iron- and carbon-based colloidal carriers for trace metals in a freshwater assessed using flow field-flow fractionation coupled to ICPMS. *Geochimica et Cosmochimica Acta* **2003,** *67*, (20), 3791-3802.
S24. Pokrovsky, O. S.; Schott, J., Iron colloids/organic matter associated transport of major and trace elements in small boreal rivers and their estuaries (NW Russia). *Chemical Geology* **2002,** *190*, (1-4), 141-179.
S25. Stolpe, B.; Guo, L.; Shiller, A. M.; Aiken, G. R., Abundance, size distributions and trace-element binding of organic and iron-rich nanocolloids in Alaskan rivers, as revealed by field-flow fractionation and ICP-MS. *Geochimica et Cosmochimica Acta* **2013,** *105*, 221-239.
S26. Ilina, S. M.; Lapitskiy, S. A.; Alekhin, Y. V.; Viers, J.; Benedetti, M.; Pokrovsky, O. S., Speciation, Size Fractionation and Transport of Trace Elements in the Continuum Soil Water–Mire–Humic Lake–River–Large Oligotrophic Lake of a Subarctic Watershed. *Aquatic Geochemistry* **2016,** *22*, (1), 65-95.